# A Numerical Study of the Eastern Tropical Pacific Ocean and the Evolution of the Costa Rica Dome

馬谷, 紳一郎

https://doi.org/10.11501/3054246

出版情報：九州大学, 1990, 理学博士, 論文博士
バージョン：
権利関係：

# A Numerical Study of the Eastern Tropical Pacific Ocean and the Evolution of the Costa Rica Dome

馬谷　伸一郎

1

# A Numerical Study of the Eastern Tropical Pacific Ocean and the Evolution of the Costa Rica Dome

by

Shin-ichiro Umatani

Research Institute for Applied Mechanics

Kyushu University, Japan

November 1990

CONTENTS

## ABSTRACT

In order to obtain a coherent picture of the eastern tropical Pacific ocean off Central America, a 3-dimensional ocean regional circulation model with a fine horizontal resolution of 0.25° x 0.25° is developed. The model is driven by the Hellerman-Rosenstein's monthly mean climatological wind stress. Several important conclusions useful to judge past conflicting hypotheses about the Costa Rica Dome and to organize the results of observations in the eastern tropical Pacific off Central America are obtained.

The model Costa Rica Dome evolves in late spring off the Gulf of Papagayo and matures in summer and early fall in accordance with strengthening of the North Equatorial Counter Current (NECC) due to the northward migration of the Intertropical Convergence Zone (ITCZ). The cyclonic turn of the NECC off the coast of Central America is found to be mainly responsible for the maintenance of the model Costa Rica Dome in summer and early fall. In winter strong northerlies converging the southernmost ITCZ from three passes in Central America excite three noticeable warm anticyclonic gyres confined to the upper layer, each of which is accompanied initially by comparatively weak cyclonic circulations with strong upwelling generated by the local wind stress curl. The model Costa Rica Dome is eroded by the warm gyres propagating westward, and thus decays in winter and early spring. The present results are remarkably consistent with the data available at present except that the values of sea water temperature in the Dome are a little

lower than those observed.

Comparisons with the results of global Pacific ocean models show that the influence of the artificial boundaries imposed in the present regional model throughout this study is negligible except for near the equator. Additional experiments clarify that the meridional migration of the ITCZ is the most important factor to understand the annual evolution of the Costa Rica Dome.

## 1. Introduction

The understanding of the tropical Pacific ocean has been improved tremendously through the development of numerical simulations. The numerical models have allowed us to develop a unified understanding of the Pacific ocean on the basis of the results obtained from the ocean observations of numerous studies. However, the numerical researches (e.g. Busalacchi and O'Brien, 1980; Philander et al., 1987; Rosati and Miyakoda, 1988) have been mainly focused on global scale phenomena and variations. These models had relatively coarse resolutions mainly due to the limitations of computer facilities, but have been rapidly improved recently. In this study, behaviors of the eastern topical Pacific ocean are investigated in detail by using a high resolution ocean regional circulation model (ORCM) adapted from the ocean general circulation model (OGCM) of the Geophysical Fluid Dynamics Laboratory (GFDL).

The eastern tropical Pacific is one of the most interesting regions among the world oceans. It is of particular interest, not only in view of the large-scale ocean-atmosphere interactions, the El Niño events, which is most conspicuous along the coast of South America (e.g. Philander, 1983; Yamagata, 1986), but also in view of the mysterious dome-like area of upwelling off the coast of Costa Rica (Cromwell, 1958). Called the Costa Rica Dome, it is an important area as a tuna fishery, however, the generation and maintenance mechanisms of the Dome were not clarified. It is the

large upwelling area, providing biologically rich (also nutrient rich) water, where a strong tropical thermocline comes near the surface due to active ocean upwelling (Wyrtki, 1964; Broenkow, 1965; Thomas, 1979). The center of the dome is located near 8 - 10° N and 88 - 90° W, with the diameter varying from 200 to 400 km (Fig.1). The above picture is mainly based on cruise observations made in fall and winter.

Two extremely different hypotheses have been proposed to explain this mysterious phenomenon. According to Wyrtki (1964), the cyclonic circulation around the Dome is determined by the North Equatorial Countercurrent (NECC)in the south, the Costa Rica Coastal Current in the east, and parts of the North Equatorial Current (NEC) in the north. That is, the Dome is considered to be one component of the northeastern tropical Pacific circulation system. This hypothesis is supported by recent oceanographic observations made in summer (Barberan et al., 1985). Their conclusion is that the large upwelling area is not induced by local atmospheric forcing but is a consequence of induced water column stretching within a cyclonic turn at the eastern end of the NECC. On the other hand, Hofmann et al. (1981) proposed that the upwelling in the dome is seasonal and induced only in summer by the localized cyclonic wind stress curl. Their hypothesis is based on the results of a simple numerical model driven by monthly mean Florida State University (FSU) wind data (Goldenberg and O'Brien, 1981). They concluded that the Costa Rica Dome is an oceanic response to seasonal local winds in summer and exists during summer

and fall.

Central America is noted also as a unique region in meteorology (Hurd, 1929; Roden, 1961; Stumpf, 1975; McCreary et al., 1988; Clarke, 1988). In winter, the atmospheric southward pressure gradient which develops between the Gulf of Mexico and the Pacific region drives strong jet-like northerlies through three passes in Central America, the Isthmus of Tehuantepec, Nicaragua's lake district, and the Panama Canal (Fig.2). Roden (1961) described the response of the ocean to a Tehuantepecer, one of the above northers. The winds move the water southward causing considerable mixing along the wind axis due to entrainment of the water from the sides and below. This process cools the sea surface temperatures (SST) by several degrees, not only in the Gulf of Tehuantepec but also farther offshore.

In this area, distinct seasonal ocean variations are found. Along the coast of Central America, strong upwelling cold regions are observed in winter (Roden, 1961). Recent satellite infrared imagery of the SST has made up for the lack of systematic oceanographic observations both in space and time. Stumpf (1975), Stumpf and Legeckis (1977) and Clarke (1988) reported that the evolution of the SST is associated with wind-induced upwelling in the winter near the Gulfs of Tehuantepec and Papagayo (Fig.3). These results are consistent with Roden's cruise observations. In particular, they all noticed the active anticyclonic gyre formation along the western edge of the jet-like northerlies. Off the Gulfs of Papagayo and Tehuantepec, the gyres are formed during winter and

early spring, after which they move westward (Stumpf and Legeckis, 1977). They have long lives of three months or more and are called Tehuantepec gyre (TG) or Papagayo gyre (PG). Stumpf and Legeckis (1977) concluded that the anticyclonic gyres propagating westward (Fig.4) are generated by local winds in Central America with an annual cycle that is most active through November to March. Matsuura and Yamagata (1982) introduced Intermediate Geostrophic (IG) dynamics to explain the longevity of these anticyclonic gyres. McCreary et al. (1988) tried to explain this predominance of the anticyclonic gyre in terms of mixed-layer physics.

Many oceanographically important and interesting phenomena are found off Central America. However, the interrelationship among them has not been well understood. The lack of a unified understanding of the phenomena observed in this area may be partly attributable to sketchy cruise observations that only provide low resolution images in time and space scales, in contrast to the rather detailed satellite images of the SST. Also, it may be partly attributable to seasonal changes of the oceanic conditions associated with the seasonal migrations of the ITCZ, as seen clearly in the wind field.

In the present study, above mentioned several unsolved problems regarding the Costa Rica Dome, the formation of the coastal upwelling, and those of the TG and PG are investigated. A coherent picture of the seasonal variation in this area is described as a response to the wind field variation. One purpose of this study is to develop the coherent picture of high seasonal

variability through the use of a high resolution numerical model.

In section 2, governing equations and views of the model used in this study are described. In section 3, the high resolution regional ocean circulation model is integrated for the eastern tropical Pacific ocean by using monthly averaged climatological wind stresses (Hellerman and Rosenstein, 1983) which resolve the ITCZ movement. The comparison of the model results with observations in the studied area is described in section 4. In section 5, the results of global Pacific ocean models are compared with those of the present high resolution regional ocean model. In Section 6, the generation of the Costa Rica Dome and the role of wind in its evolution are studied. Also shown are how and which winds are responsible for the generation and maintenance of the Costa Rica Dome. In the final section, section 7, the summary and concluding remarks are described.

## 2. Description of the model

The numerical model used in this study is based on the OGCM developed at GFDL. The model was tuned to have a fine horizontal resolution of 0.25° x 0.25° in order to study the variation of the eastern tropical Pacific ocean in detail. Lateral artificial boundaries at the northern, southern and western walls are imposed to OGCM of GFDL, hence the model used in this study is a three dimensional ORCM. Artificial boundaries influence the model results in describing the real ocean, if appropriate boundary conditions are not used. At the artificial boundaries, high viscous buffer layers are imposed to weaken the influence of these boundaries. When the model has an artificial eastern boundary, we have to use proper boundary conditions (e.g. open boundary conditions), in order to describe the influence of the Rossby waves moving westward into the interior region. Since this model does not have an artificial eastern boundary, the most serious Rossby wave's influence is negligible. As demonstrated by Cane (1979) and Philander and Pacanowski (1981), current systems in the studied eastern tropical Pacific are basically simulated by use of the wind forcing of this area. Their results suggest that oceanic conditions in this studied area will be simulated in the present regional model.

The first version of the GFDL OGCM was coded more than 20 years ago (Bryan and Cox, 1967), and the model was made efficient for a modern computer by Cox (1984). The details of the physics

and numerics are described in Bryan (1969). In this chapter, the 3-dimension numerical ocean model is briefly described, after which the adopted physics and numerical methods used in this regional model are discussed.

## 2.1 Governing equations

The model is a continuous stratified three dimensional ocean model. The Navier-Stokes equation on the spherical co-ordinate system with three basic assumptions is used. The first assumption is the Boussinesq approximation, which neglects density variations except in the buoyancy term. The second is a hydrostatic approximation that eliminates the vertical acceleration term from the vertical momentum equation. The third is the turbulent viscosity hypothesis which assumes the turbulent mixing larger than the molecular mixing and parameterizes the effect of sub-grid fluid motion on the momentum transport. A rigid-lid assumption is made for the purpose of efficient computation, and the assumption eliminates high speed external gravity waves.

Temperature variation is described by the conservation equation of heat (internal energy) as mentioned later. The term of temperature is also used to imply potential temperature. The difference between the two quantities is relatively small in the ocean, and either use of them does not significantly alter the computation of horizontal density gradients in determining the velocity field (e.g. Knauss, 1978). Salinity is an important variable in the ocean, however, in this model it is assumed to be a

constant value of 35.0. This is because it is difficult to estimate salt flux across the surface boundaries with enough resolution in time and space.

Let,

$$m = \sec\phi$$
$$n = \sin\phi$$
$$f = 2\Omega\sin\phi \qquad (1)$$
$$u = \frac{a}{m}\frac{d\lambda}{dt}$$
$$v = \frac{a}{m}\frac{d\phi}{dt},$$

where $\phi$ is latitude, $\lambda$ is longitude and a is the radius of the earth. The density of water is $\rho = \rho_0 + \rho'$, where $\rho_0$ is a constant, standard density. The equations of motion are written as follows;

$$u_t + L(u) - fv = -ma^{-1}(p/\rho_0)_\lambda + F^u \qquad (2)$$
$$v_t + L(v) + fu = -a^{-1}(p/\rho_0)_\phi + F^v, \qquad (3)$$

where the advection operator L for any scalar quantity x is defined as

$$L(x) = ma^{-1}[(ux)_\lambda + (vm^{-1}x)_\phi] + (wx)_z, \qquad (4)$$

and $F^u$ and $F^v$ represent the turbulent mixing terms.

The hydrostatic equation is

$$\rho g = -p_z \ , \tag{5}$$

where g is the gravitational acceleration.

The continuity equation and the conservation equation of heat is

$$L(1) = 0 \tag{6}$$

$$T_t + L(T) = q \ , \tag{7}$$

where q is the turbulent mixing term.

The equation of state has the form of

$$\rho = \rho( T, S, z), \tag{8}$$

where T is potential temperature and S is salinity having a constant value of 35.0. The depth dependence is due to the compression effects. In this model Eq.(8) is represented by a 9-term, third-order polynomial, of which coefficients are determined for each vertical level to fit the Knudsen formula (Bryan and Cox, 1972).

The turbulent mixing terms in Eqs (2), (3) and (7), $F^u$, $F^v$ and q are written as follows,

$$F^u = A_V u_{zz} + A_H a^{-2}[\ \nabla^2 u - (1+m^2n^2)u - 2nm^2 v_\lambda\ ] \tag{9}$$

$$F^v = A_V v_{zz} + A_H a^{-2}[-\nabla^2 v + (1+m^2n^2)v - 2nm^2 u_\lambda\ ] \tag{10}$$

$$q = ((K_V/\delta)T_z)_z + K_H a^{-2}\nabla^2 T\ , \tag{11}$$

where $A_H$ and $K_H$ are the coefficients of horizontal viscosity and diffusion respectively, $A_V$ and $K_V$ are the corresponding vertical coefficients, and $\nabla^2$ is the horizontal Laplacian operator defined by

$$\nabla^2 x = m^2 x_{\lambda\lambda} + m(x_\phi/m)_\phi\ . \tag{12}$$

Vertical mixing is known to have a complex dependence on the vertical stability, in other words, it depends on the vertical density stratification and vertical shear. $A_V$ and $K_V$ are accurately estimated by considering the stability dependence in the following forms (Robinson, 1966; Jones, 1973; Pacanowski and Philander, 1981).

$$A_V = \frac{A_0}{(1+\alpha R_i)^k} + A_b \tag{13}$$

$$K_V = \frac{A_V}{1+\alpha R_i} + K_b\ , \tag{14}$$

and the Richardson number is defined by

$$R_i = -\frac{g}{\rho_0}\frac{\partial \rho}{\partial z}/(u_z^2 + v_z^2), \tag{15}$$

where $A_b$ and $K_b$ are background mixing parameters representing the values in the case, $R_i \rightarrow \infty$ . Pacanowski and Philander (1981)

studied the effects of the parameterized vertical mixing in numerical models and proposed to adopt the values of constants in Eqs (13) and (14) as follows,

$$
\begin{aligned}
A_b &= 1 \ cm^2 sec^{-1} \\
K_b &= 0.1 \ cm^2 sec^{-1} \\
k &= 2 \\
\alpha &= 5 \\
A_0 &= 50 \ cm^2 sec^{-1}.
\end{aligned}
\tag{16}
$$

In this model, these parameterized vertical turbulent mixing coefficients are adopted for all stable stratification. For unstable stratification, the vertical diffusion q is assumed to be infinite, namely a convective adjustment is used. Let $\rho'_z$ be the local vertical density gradient, then $\delta$ in Eq.(11) is determined as follows,

$$
\delta = \begin{cases} 1 & (\rho'_z < 0) \\ 0 & (\rho'_z > 0). \end{cases}
\tag{17}
$$

The lateral walls are non-slippery, adiabatic walls, so that the boundary conditions at lateral walls are,

$$
u, \ v, \ T_n = 0 \ , \tag{18}
$$

where the subscript, n indicates a local derivative normal to the wall.

Upper boundary conditions at z = 0 are,

$$w = 0$$
$$\rho_0 A_V(u_z, v_z) = (\tau^\lambda, \tau^\phi) \qquad (19)$$
$$K_V T_z = Q/\rho_0 C_o ,$$

where $\tau^\lambda$ and $\tau^\phi$ are zonal and meridional components of surface stresses, respectively, Q is a surface heat flux, and $C_o$ is the specific heat of sea water.

At the bottom, $z = -H(\lambda, \phi)$,

$$w = -mua^{-1}H_\lambda - va^{-1}H_\phi$$
$$\rho_0 A_V(u_z, v_z) = (\tau_B^\lambda, \tau_B^\phi) \qquad (20)$$
$$T_z = 0 ,$$

In this model $\tau_B^\lambda$ and $\tau_B^\phi$ are assumed to be zero, then the bottom is slippery and adiabatic.

**2.2 Numerical methodology**

The governing equations with the boundary conditions are solved by finite difference methods. The grid configuration is a staggered 'B' grid (Arakawa and Lamb, 1977), and the time differencing is a centered, leap-frog scheme. The model conserves total (kinetic plus potential) energy. The details of the finite difference equations are found in Bryan (1969) and Cox (1984).

The eastern tropical Pacific ocean model used in this study

extends from 115° W to 75° W in longitude and from 10° S to 20° N in latitude, and is bounded by the American continent in the east. The model topography is shown in Fig.5. The numbers in the figure represent the number of vertical levels. The horizontal grid intervals are 0.25° in both longitude and latitude. The model has 11 levels in the vertical, with 5 levels in the top 110 m to resolve the upper ocean in detail. The vertical grid scheme is shown in Fig.6. The dashed lines indicate levels at which the temperature (T) and the horizontal velocity (**V**) are defined, and the vertical velocity (w) and Richardson number ($R_i$) are located on the solid line levels. The actual topography and geometry data are fitted to the nearest vertical levels of the model. Depths less than 10 m, and the Atlantic ocean, are assumed to be a land area. The maximum ocean depth is taken as 4310m. The vertical resolution may not be high, in particular beneath the 150 m level.

The coefficients of horizontal diffusion ($A_H$) and dissipation ($K_H$) are fixed to constant values, $2 \times 10^7$ $cm^2sec^{-1}$ and $10^7$ $cm^2sec^{-1}$, respectively. In order to weaken the effects of artificial lateral boundaries, coefficients are multiplied by twenty to the north of 17.5° N, and to the south of 7.5° S. From 105° W to the western boundary at 115° W, they are gradually increased by one to twenty times of the values in the interior region. Light shaded regions in Fig.5 indicate the high viscous buffer region.

## 2.3 External forcings

In general, oceanic motions are induced by the surface wind stress and surface heat flux. These are external forcings that have to be estimated by the atmospheric and oceanic conditions. In this model, however, the wind stress is imposed based on the observed wind stress data (Hellerman and Rosenstein, 1983). On the other hand, a surface heat flux is calculated using the simulated SST and observed wind speed data. This is because available heat flux data are less accumulated compared with the wind data, and do not have an enough resolution of time and space to use in this model. It is also because realistic seasonal variations of the tropical Pacific ocean could be obtained by the same method of heat flux estimation (Philander et al., 1987). It is assumed that the variation of the surface heat flux is caused by that of the simulated SST and the wind stress, however, the result of Reed (1985) showing that the seasonal variation of SST is caused by variations of surface heat flux suggests that the method of heat flux estimation must be improved in the near future.

### (a) Momentum flux

On the surface, momentum fluxes are expressed by the wind stresses (Eq.19). They are calculated by the bulk aerodynamic formula as follows,

$$\tau^{\lambda} = \rho_a C_D u_a V_a$$
$$\tau^{\phi} = \rho_a C_D v_a V_a \quad , \qquad (21)$$

where $\rho_a = 1.2 \times 10^{-3}$ g cm$^{-3}$ is the air density, $C_D$ is the exchange coefficient for momentum, $u_a$ and $v_a$ are the zonal and meridional components of wind velocities, respectively, and $V_a$ is surface wind speed defined by $V_a=(u_a^2 + v_a^2)^{1/2}$.

The monthly averaged climatological wind stress data are given by Hellerman and Rosenstein (1983). The data used in this model are their updated data having a 1° x 1° resolution in both longitude and latitude. They calculated the wind stress by using over 35 million surface observations covering the world's oceans for the period from 1879 to 1976. The $C_D$ is considered to be a function of a wind speed and of the air and sea surface temperature difference, and is approximated by a polynomial of the second order in the wind speed and stability (Hellerman and Rosenstein, 1983).

**(b) Heat flux**

The surface heat flux, Q, in Eq.(19) is expressed by

$$Q = Q_S - Q_L - Q_E - Q_H, \qquad (22)$$

where Q is the total (net) heat flux into the ocean, $Q_S$ is a net downward heat flux of the solar radiation, (the insolation minus reflected short-wave radiation), $Q_L$ is a net upward heat flux due to the long-wave radiation, $Q_E$ is a latent heat flux, and $Q_H$ is a sensible heat flux. Empirical bulk formulae are used to estimate the flux in the air-sea heat exchange. The $Q_S$ depends on the time of a year, latitude, and cloudiness; $Q_L$ depends on SST, air vapor

pressure, and cloudiness (Reed, 1985). However, in this model they are fixed to the constant values, $Q_S$ = 500 ly/day (ly = cal/cm$^2$) and $Q_L$ = 115 ly/day. These values are adopted from the zonal and annual mean values, which do not have substantial latitudinal variations in the tropics (Haney, 1971; Philander et al., 1987). The effects of cloudiness and air vapor pressure are included in these constant values.

The latent heat flux, $Q_E$ is given by,

$$Q_E = \rho_a C_D V_a L[e_s(T_o) - \gamma e_s(T_a)](0.622/P_a), \qquad (23)$$

and the sensible heat flux, $Q_H$ is,

$$Q_H = \rho_a C_D C_p V_a (T_o - T_a), \qquad (24)$$

where the atmospheric pressure $P_a$ = 1013 mb; the latent heat of condensation L = 595 cal $g^{-1}$; the drag coefficient $C_D$ is assumed to be a constant, 1.4 x $10^{-3}$; the specific heat of air $C_p$ = 0.24 cal $g^{-1} \cdot C^{-1}$; $T_o$ is the sea surface temperature; $T_a$ is the atmospheric temperature at the surface; $\gamma$ is the relative humidity which is assumed to be 0.8. The saturated vapor pressure $e_s$ for K in the absolute Kelvin temperature unit is given by

$$e_s(K) = 10^{(9.4051 - 2353/K)}. \qquad (25)$$

On the basis of Philander and Seigel (1985)'s work, $T_a$ is always

assumed to be 1.5°C less than the predicted sea surface temperature, $T_o$. Also, the surface wind speed $V_a$ in the formulae for $Q_E$ and $Q_H$ is assumed to be greater than or equal to 4.8 m/sec, so that the effect of high frequency wind fluctuation which is absent from the mean monthly winds is taken into account.

**2.4 Procedure of integration**

The initial condition is a climatological annual mean of the temperature fields (Levitus, 1982) with no currents. Levitus datasets are based on monthly analyses of station data, expendable bathythermography (XBT) data, and mechanical bathythermography (BT) data on files at the National Oceanographic Data Center (NODC). The data with 33 vertical levels are averaged over a 1° x 1° area. The observation periods are from 1901 to 1978. The temperature data is interpolated to set the initial temperature distribution in the model. The initial temperature fields at depths of 10 m and 50 m are presented in Fig.7. Though there are no currents in the initial instance, a geostrophic adjustment process produces a basic current system in a few inertial periods.

The model is integrated with the external forcings for four years, which is considered to be an enough period for the model to reach an equilibrium state (Philander and Seigel, 1985). The results from the fourth year are discussed in this study.

## 3. Climatological monthly mean wind forcing experiment

In this section, the model is driven by the climatological monthly mean wind stress compiled by Hellerman and Rosenstein (1983). The winds in the studied area, in particular north of the Equator, have distinct seasonal variability (Fig.8). During winter and spring, northers and north-easterly winds are prominent off Central America. In contrast, during summer and fall, southerly and south-westerly winds are distinct in the south of 10°N. They vary in accordance with the meridional migration of the ITCZ. It is noteworthy that the northers blowing over Central America take three passes (Fig.2), making three dipole-like structures of wind stress curl (Fig.9).

### 3.1 Surface currents and temperatures

Figure 10 shows the annual march of surface currents (at a depth of 10 m, the center depth of the most upper layer), as simulated in the present model. As is well known, there are three major components of lateral surface circulation in the eastern tropical Pacific. They are the westward-flowing South Equatorial Current (SEC) near the equator, the eastward-flowing North Equatorial Countercurrent (NECC) near 5°N, and the westward-flowing North Equatorial Current (NEC) north of 10°N (e.g. Wyrtki, 1967). These currents are well simulated in the model, and show high seasonal variability due to seasonal changes of the surface winds associated with the meridional migrations of the ITCZ.

Through May to December, the northward trade winds are intense (Fig.8). In particular, they are most intense during the boreal fall because the ITCZ is located farthest north at that time. Through January to April, however, these trade winds diminish with the southward movement of the ITCZ. In accordance with these wind changes, the simulated NECC intensifies in summer and fall, reaching the eastern end of the Pacific basin. During winter and spring, however, the simulated NECC diminishes and shows high variability. The variations of the NECC are consistent with the numerical results by Philander et al. (1987) and with the observed results based on monthly sea level data at island stations (Wyrtki, 1974).

Through December to March, winds from the Gulf of Mexico are persistent and intense north of 5°N as referred to in section 1. In particular, the three passes in Central America are clearly resolved in the Hellerman-Rosenstein wind fields (Fig.8) as compared to the monthly mean climatology of the FSU winds compiled by Goldenberg and O'Brien (1981). These strong, jet-like northerlies are associated with three dipole-like structures of the wind stress curl (Fig.9), and excite three noticeable anticyclonic circulations associated with comparatively weak cyclonic circulations off the coast of Central America (see the simulated February result in Fig.10). The predominance of the anticyclonic circulations is discussed in the next sub-section. Thus, in winter, the simulated westward current near 10°N shows a complicated meandering pattern.

Figure 11 shows simulated surface temperature distributions (at a depth of 10 m). In December, a swirl pattern of temperature associated with the anticyclonic Tehuantepec gyre is excited off the Gulf of Tehuantepec by the Tehuantepecer. A similar, but much weaker pattern is simulated off the Gulf of Papagayo also in winter. A warm tongue generated off Panama in winter elongates southwestward and, in June, evolves into a zonally elongated warm patch associated with the anticyclonic surface circulation just north of the equator. The wavy front south of this warm patch reminds us of the long waves found farther westward as described by Philander et al.(1985).

The simulated Costa Rica Dome evolves off the Gulf of Papagayo in spring and matures in summer and early fall. In late fall and winter it fades out and the more variable gyres forced by the northers take its place. The center of the simulated Dome is located near 10° N, 90° W, with the temperature in the core less than 26° C. The diameter is about 300 - 500 km in early summer, although in fall the Dome elongates in the zonal direction. These structures are remarkably consistent with those observed (Wyrtki, 1964; Broenkow, 1965; Thomas, 1979). It is noteworthy that the Costa Rica Dome becomes prominent as the ITCZ reaches farthest north in the boreal fall (Fig.8). In contrast to the hypothesis of Hofmann et al. (1981), the present model results show that the global meridional trade winds that converge into the ITCZ are most responsible for its existence. This is further confirmed by the simulated result that the center of the Dome is located about 500

km west of the center of the cyclonic curl of the wind stress associated with the ITCZ in summer (Fig.9, see also Fig.13).

### 3.2 Subsurface currents and temperatures

#### (a) Anticyclonic gyres off Central America

Figures 12 and 13 show the annual march of the subsurface (at a depth of 50 m) currents and temperature distributions, respectively. Three warm anticyclonic gyres off the coast of Central America are clearly seen in winter (January through March), even though the curl of the wind stress has a dipole-like structure above the three regions during that period (Fig.9). The anticyclonic gyres, in particular those generated off the Gulfs of Tehuantepec and Papagayo, are confined to above the sharp thermocline existing at a depth of about 100 m (Fig.14; for the gyre off the Gulf of Papagayo). It is found that their upper layer thickness anomaly is large. In addition, they propagate westward faster than the long Rossby wave speed, about 0.05 m $sec^{-1}$ as estimated for the same latitude, 11°N. For example, the Papagayo gyre generated in December preserves its identity for a few months and propagates westward at a speed of about 0.1 m $sec^{-1}$ which is almost twice as fast as the long Rossby wave speed. As suggested in Matsuura and Yamagata (1982), and more recently in McCreary et al. (1988), the large upper layer thickness anomaly associated with the gyre may partly explain the excessive propagation speed.

In summary, it is reasonable to expect that the coherent anticyclonic gyres generated in winter off the coast of Central America

are in the dynamical balance between the planetary wave dispersion and the nonlinear planetary geostrophic divergence related to the finite amplitude upper layer thickness anomaly. In other words, it is quite possible that they are governed by the intermediate geostrophic (IG) dynamics found by Charney and Flierl (1981), and Yamagata (1982) (see also Matsuura and Yamagata, 1982; Williams and Yamagata, 1984). Taking L = 200 km as a radius of the gyre, the Coriolis parameter $f = 3 \times 10^{-5}$ $sec^{-1}$, the dimensional beta parameter $\beta = 2 \times 10^{-11} m^{-1} sec^{-1}$, the Rossby's internal radius of deformation $L_R = \sqrt{g^* H}/f = 50$ km ($g^*$: reduced gravitational acceleration, H: upper layer thickness) and $U = 0.2$ m $sec^{-1}$, the estimation of three nondimensional parameters, the beta parameter $\hat{\beta}$, Rossby number $\epsilon$ and stratification parameter s, gives about 0.1, 0.03 and 0.1, where

$$\hat{\beta} = \beta L/f, \ \epsilon = U/(fL), \ s = L_R^2/L^2.$$

The estimation satisfies the conditions of the IG dynamics,

$$\epsilon \sim \hat{\beta}^2, \text{ and } s \sim \hat{\beta}.$$

The simulated anticyclonic gyres in the model are induced by the monthly mean wind stress having no variability in a shorter time, however, the observed Papagayo gyre (PG) and Tehuantepec gyre (TG) (see Fig.2) are considered to be forced by gusts blowing during winter (Stumpf and Legeckis, 1977; McCreary et al., 1988). Figures 15a and 15b show the vertical velocity profile of the gyres as observed and simulated off the Gulf of Papagayo. The both gyres are active in an upper layer shallower than about 100 m, the depth

of their thermocline. Although the details of the way to generate gyres are not the same, the behavior and structures of generated gyres are quite similar. It is much of interest to estimate the integrated magnitude of the wind stress for both the simulated and observed gyre. However, the estimation is difficult, in particular for the observed gyre because of the lack of the short-period (at least a few days) wind data covering the Gulf of Papagayo.

Another interesting aspect to note here is that a new Papagayo gyre forms in February (Fig.13), in spite of the winds remaining almost steady in the sense of a monthly mean. This suggests that nonlinear coherent structures may be successively generated under the almost steady supply of potential vorticity through the wind stress curl.

**(b) Variability of the Costa Rica Dome**

The Costa Rica Dome is clearly seen in the subsurface temperature field (Fig.13). The Dome is generated in early spring, and evolves in summer and fall and elongates in the zonal direction. The annual evolution of temperature at a depth of 50 m along 9°N (Fig.16) shows that the Dome is generated at about 88°W in spring, and that after May it propagates westward with a speed of about 0.05 m $sec^{-1}$, almost that of the long Rossby wave. After maturing in fall it weakens in winter and spring, being eroded by the warm anticyclonic gyres that are propagating westward at a speed of about 0.1 m $sec^{-1}$.

The meridional section along 95°W of the zonal current in the

model (Fig.17) shows that the eastward NECC develops in the upper 50 m and expands to between 2° N and 10° N, and that the broad westward NEC is located north of 10° N. In winter and spring the NECC becomes more confined to near 5° N, and the more confined westward current appearing near 10° N has a deeper structure as a southern flank of the anticyclonic Papagayo gyre. It should be noted that the calculated zonal velocity fields near the equator in summer correspond well with the measurements at the same longitude during 11-15 June, 1981 (Fig.18a) and during 2-5 August, 1980 (Fig.18b). It is known that during these years the Pacific was not affected by El Niño and that the tropical Pacific ocean well reflected the climatological conditions. This model can well simulate the Equatorial Undercurrent (EUC) even though the model is a regional one.

The temperature zonal section along 10° N (Fig.14) shows that there is some difference between the Dome in spring and in summer. In the generation stage of the Dome from January to March, the cold region located at about 88° W is relatively small and is evident in the upper layer. In contrast, in the mature stage from July to September, the cold Dome is elongated in the zonal direction and it exists from the surface to beneath 200 m. This suggests that in the early stage the Dome is generated mainly by local cyclonic wind stress curl acting on the surface, and that in the mature stage it is not maintained by the local wind stress curl. The hypothesis proposed by Hofmann et al. (1981), "The upwelling in the Dome is seasonal and induced in summer by the localized cyclonic wind

stress curl.", is not consistent with this result. Another hypothesis proposed by Wyrtki (1964) agrees with this result, in particular in the mature stage. This is discussed in more detail in the next subsection.

### 3.3 Mass and heat budgets of the Costa Rica Dome

In order to calculate the mass and heat budgets off the coast of Costa Rica during different seasons, two artificial boxes, A and B, are considered in the upper 60 m off Central America. Box A has a rectangular domain bounded by 86.5°W, 88.5°W, 8°N, and 10°N, which covers the cyclonic circulation in winter located off the Gulf of Papagayo. The other box, B, is also a rectangular domain bounded by 89°W, 91°W, 9°N, and 11°N, which covers the central part of the Costa Rica Dome during its mature stage. Since the Dome is distinct in the upper layer, the adopted depth of the two boxes is sufficient to calculate the budgets. The annual variations for the heat budgets of boxes A and B are shown in Figs 19a and 19b, respectively, with area-averaged upwelling velocity and the vertical velocity estimated by the theory of the upper Ekman layer induced by the surface wind stress (Pedlosky, 1979). In Figs 20a and 20b, detailed mass and heat budgets of boxes A and B are shown. When the heat transports due to the horizontal and vertical advection are calculated, the temperatures averaged within each box are assumed as representing characteristic temperatures. Then the positive (negative) value indicates that the box is warmed (cooled).

The nearshore box A is cooled from December to April (Fig. 19a). This is mainly due to a negative heat convergence. During this period, the degree of convergence varies with strength of upwelling, and it is closely related to the vertical velocity estimated from the surface wind stress. The temperature, averaged within the box A, drops most sharply in January at a rate of -1.4 deg/month due to an active upwelling directly related to the positive curl of the wind stress. The upward mass transport at a depth of 60 m is 0.18 Sv ($Sv=10^6 m^3 sec^{-1}$) in January, which is equal to $3.7 \times 10^{-6}$ m $sec^{-1}$ in an area-averaged upwelling velocity (Fig.20a). The active cooling lasts from December to April in accordance with the existence of strong northerlies off Costa Rica (see Figs 8 and 9). This means that the active cooling is induced directly by the local wind stress curl. The situation changes totally from late spring to late summer because of the reduced local upwelling. The temperature increases due to a surface heating and lateral diffusion of heat.

The offshore box, B, is cooled from February to June (Fig. 19b). The cooling is mainly caused by the negative heat convergence. In contrast to the box A, the changes of the upwelling speed are unrelated to those of the vertical velocity estimated by the surface wind stress. The temperature, averaged within the box B, drops most sharply in May at a rate of -2.4 deg/month due to lateral advection and upwelling of cold water (Fig.20b). The upward mass transport at a depth of 60 m is 0.17 Sv in May, which is equal to $3.4 \times 10^{-6}$ m $s^{-1}$ in an area-averaged

upwelling velocity (Fig.20b). In contrast to the box A, this upwelling cannot be directly related to the local wind stress curl which is rather weak above the region (see Fig.9), but rather to vorticity stretching associated with a cyclonic turn of the NECC off the coast of Central America. This is confirmed by the mass budget (Fig.20b). In May, the mass below 60 m comes from the east at a rate of 1.04 Sv, from the west at a rate of 0.13 Sv, leaving to the north at a rate of 0.89 Sv and to the south at a rate of 0.12 Sv. Above 60 m it comes from the north, east and south at rates of 0.67 Sv, 0.61 Sv, and 0.09 Sv, respectively, but leaves to the west at a rate of 1.54 Sv. Thus, a rough estimation is that the mass comes from the east below 60 m and leaves to the west above 60 m. The resulting active upwelling lasts from April through June in accord with the strengthening of the NECC due to the northward migration of the ITCZ, and ends up when a cool dome-like area known as the Costa Rica Dome develops in summer and fall.

This is further confirmed by another experiment in which the winds of May are used and kept steady throughout the experiment. This case will be discussed in detail in section 6. This additional experiment demonstrates that the cyclonic turn composed of the NECC, the Costa Rica Coastal Current and the NEC is generated by the winds of May. The origin of the Costa Rica Dome itself can be traced back to the local upwelling off the Gulf of Papagayo in winter. However, the Dome evolves mainly due to the northeastern tropical Pacific circulation system generated by the surface wind field associated with the northward migration of the ITCZ.

From July to October the total heat budget is almost equal to zero. Heating through the surface heat flux, horizontal diffusion and vertical diffusion is balanced with the cooling effect of negative heat convergence. During this period the Costa Rica Dome has almost a constant temperature (Fig.20b), and is zonally elongated to the west (see Figs 13 and 16).

From November through January, warm water accumulates and thus reduces the cold Costa Rica Dome. In particular, the Dome is warmed at a rate of 3.2 deg/month as shown in the December calculation, and reaches the maximum temperature of 25.5°C in January (Fig.20b). This warming is associated with both downwelling, most active in November, and lateral advection of heat due to the warm gyres excited near the coast of Costa Rica. It should be noted here that the cooling due to the intense local upwelling in January, $5.3 \times 10^{-6}$ m $sec^{-1}$, is canceled by this advection of warm water associated with the westward moving anticyclonic gyre.

Figures 21a and 21b show the annual change of the temperature profile at the center of the boxes A and B, respectively. These results clearly show that in the nearshore box A, the cooling is confined to the upper layer during the generation stage of the Dome (Fig.21a), in contrast, that in the offshore box B, the Dome has a deep structure (Fig.21b) as suggested by Wyrtki (1964) in the maturing stage, which is consistent with the observations of Barberan et al. (1985). The Costa Rica Dome is not maintained by the local positive wind stress curl in summer as hypothesized by Hofmann et al. (1981), but rather it is established by the

convergence of a cold water mass associated with a cyclonic turn of the NECC off the coast of Central America as hypothesized by Wyrtki (1964).

## 4. Comparison with observations

Figure 22 compares the subsurface temperature field at a depth of 50 m produced in the model with the climatological field at the same depth prepared by Levitus (1982). The correspondence of the model results with the data is rather good except for the period of February to April. In particular, the cold Costa Rica Dome in summer and fall is simulated well with regard to the lateral scale and location. In contrast, the oceanic conditions near the equator are not well simulated. This is because the model is a regional one and cannot simulate the global thermocline east-west inclination induced by the easterly trade winds blowing throughout the Pacific ocean. This lack of correspondence is also found in the next section which compares this model with global Pacific ocean models.

The minimum temperature at the center of the simulated Dome is lower than that of the climatology by two or three degrees (Fig.22). This is because the model surface heat flux (total downward heat flux) is too small compared to the available estimates. For example, the mean surface heat flux, Q, calculated by Reed (1983) ranges from over 75 W $m^{-2}$ to around 100 W $m^{-2}$, almost twice larger than the flux of the model (Fig.23a). In the model, the value of $Q_S$-$Q_L$ is assumed to be 385 ly/day (186 W $m^{-2}$). Since the observed $Q_S$-$Q_L$ varies approximately from 170 to 200 W $m^{-2}$ (Reed, 1983), this assumption is not bad when the seasonal variation is ignored. However, it will be needed to use the

refined $Q_S$-$Q_L$, in particular $Q_S$ with enough space and time resolutions. The simulated $Q_E$ (upward heat flux) is considerably large compared to the observations (Fig.23b). Considering the annual mean value, the difference in $Q_E$ between the model and the observation is responsible for about 80 % of the difference in Q between the model and the observation. In order to simulate more reasonable values of the sea temperature, the formulae for both the solar short-wave heating, $Q_S$, and the latent heat flux, $Q_E$, need to be refined.

The correspondence of the model results with the Levitus climatology is rather poor for February - April, in particular off the Gulfs of Papagayo and Panama (Fig.22). This is not due to a model fault, but rather due to the low resolution of the climatology data. Using global area coverage (GAC) data gathered by the NOAA polar orbiting satellite, Legeckis (1988) recently summarized the positions of the fronts off Central America from March 7 to 20, 1985 (Fig.24). It is remarkable how well the location of the fronts corresponds with the model product for February - April (Fig.22). However, the results raise another question. The satellite data showing the conditions of the sea surface temperatures (SST) correspond better with the subsurface temperature fields of the model at a depth of 50 m rather than with the surface ones at a depth of 10 m. This suggests that the model simulates the interior ocean structures well, but that it is necessary to improve the upper boundary conditions, in particular heat flux estimations and upper mixed layer dynamics.

## 5. Comparison with results of global Pacific ocean models

The model used in this study has artificial boundaries in the west, north, and south, and is bounded by realistic coast lines at the eastern side. Near the first three boundaries, artificial high viscous buffer regions have been introduced to reduce the influence on the interior region. However, it is impossible to erase the effects completely. In the previous section, the model results are compared with observations, and it is shown that the present regional model simulates the observed oceanic conditions well except for in the equatorial region. In this section, the results of the regional model are compared with those of two global Pacific ocean models (Table 1).

Figure 25 shows the annual march of temperature fields at a depth of 50 m as simulated by a global model, hereafter referred to as G1 model (Masumoto, 1989, private communication). The characteristics of this global model are the same as those of the regional model except for the horizontal resolution; 0.5° x 0.5° in latitude and longitude, and the simulated area; the global Pacific, from 30° S to 30° N. It is noted that the winds used in both regional and G1 models are the same and have 1° x 1° resolution. The evolution of the Costa Rica Dome, in particular its position and variation during the year, are remarkably similar to the results of the regional model (see Fig.13). The minimum temperature of the model Costa Rica Dome in the G1 model is a little low compared with that simulated by the regional model.

This is caused by the difference of the horizontal resolution. Since the coefficient of horizontal heat mixing is the same in both models, the warming effect of the horizontal mixing on the cold Dome is larger in the regional model with its finer horizontal grid spacing than in the G1 model.

The fine temperature structures along the coast of Central America during winter and spring are also simulated much like those in the regional model. Three distinct anticyclonic gyres evolve through a similar process, however, the influence of the resolution difference between the two models is found in the shape of the gyre off the Gulf of Papagayo. The high resolution regional model resolves two temperature maxima off the Gulf of Papagayo in February and March, but the coarse resolution G1 model does not resolve the structure. The regional model partly simulates the isolated warm gyre related with the PG (Fig.4), however, the G1 model does not.

In vicinity of the equator, the correspondence of temperature distribution is poor in the regional model (left panel in Fig.22). The temperature simulated in the regional model is too warm near the equator. This is because the global east-west inclination of the thermocline is not simulated in the regional model as was described in the previous section. The G1 model well simulates the temperature distributions except for the temperature values themselves.

The influence of the artificial boundaries set in the regional model is negligible except for the southern one. Its influence is

interrelated with that of the thermocline inclination, described previously, and cannot be estimated independently.

Figure 26 shows temperature distributions at a depth of 48 m as simulated in another global model, hereafter referred to as G2 model, having horizontal resolution of 1/3° in latitude and 0.5° in longitude (Gordon, 1990, private communication). The latitude resolution is finer than that of the G1 model. The Costa Rica Dome is also well simulated in this G2 model. However, the fine structures of the Dome and those along the coast of Central America are not well simulated. This is mainly because the G2 model is driven by coarse resolution wind fields (2° x 2°). The G1 model having a coarser horizontal resolution than the G2 model well simulates the fine structures consistent with observations (Fig.24). The fine resolution of the wind stress, one of the external forcing, affects the simulated results efficiently.

The flat bottom topography is adopted in the G2 model, which well simulates the Costa Rica Dome. Hence, it is clear that the hollow basin found off the Gulf of Papagayo (see Fig.6) has no effect on the existence of the Costa Rica Dome.

## 6. Role of wind in the evolution of the Costa Rica Dome

It has been shown in previous sections that the annual evolution of the Costa Rica Dome is well simulated when the climatological monthly mean wind stress is used. The results of the simulation are consistent with observations. The analysis of the results suggests that the meridional migration of the ITCZ, which causes the characteristic wind fields in the eastern tropical Pacific ocean, is essential to the evolution of the Costa Rica Dome. Due to the migration, two distinct winds alternate seasonally in this area (Fig.8). One is a strong jet-like northerly wind during winter (Hurd, 1929; Roden, 1961; Clarke, 1988) that causes coastal upwelling and induces meso scale warm gyres (Stumpf, 1975; Stumpf and Legeckis, 1977; McCreary et al., 1988; Legeckis, 1988). The other is a southerly wind blowing from the southern hemisphere over the equator into the ITCZ with its northward migration during summer and fall (Fig.8). Cane (1979) and Philander and Pacanowski (1981) showed that this southerly wind causes a countercurrent near the equator. In section 3, it was suggested that these winds play important roles in the generation and the maintenance of the Costa Rica Dome. In this section, the role of these winds in the oceanic response to the evolution of the Dome is described.

### 6.1 Methods

The model used in these experiments is the same as that used

in section 3 except for the forcing wind fields. In Section 3, monthly mean winds (MMW) are used to force the model, hereafter this experiment is referred to as EX0. In this section, January wind (JANW) and May wind (MAYW) are used as forcing winds (Fig.8). Fixed JANW is used in EX1, and fixed MAYW in EX2. In EX3 - EX7, the importance of both the northerly and the southerly winds in the evolution of the Dome is emphasized by switching the MMW, JANW and MAYW in various manner. Using JANW as a typical one of the northerly winds, and MAYW as that of the southerly winds, numerical simulations are carried out and the results are compared to those of EX0. In particular, we note the results for September, the mature stage of the Costa Rica Dome, and those for May when the relatively small but clear Costa Rica Dome is found and when the cooling rate caused by upwelling in the Costa Rica Dome area is the largest during a year (see Fig.19b).

The experiments carried out in this section are as follows and they are shown in Table 2.

EX1 : The model forced by fixed JANW.

EX2 : The model forced by fixed MAYW.

EX3 : The forcing winds switched from MMW to JANW on January 15th in the fourth year.

EX4 : The forcing winds switched from JANW to MMW on January 15th in the fourth year.

EX5 : The forcing winds switched from MMW to MAYW on May 15th in the fourth year.

EX6 : The forcing winds switched from MAYW to MMW on May 15th in

the fourth year.

EX7 : The model forced by JANW from January to April, and MAYW from May to December.

The integrations are carried out over three years to spin up the model ocean which is initially at rest. The results are shown as temperature fields at a depth of 50 m after this spin up period. The forcing winds in experiments EX3-EX7 change gradually over a period of one month from the first wind fields to the second as mentioned above.

### 6.2 Results

Figures 27a and 27b show the quasi-steady temperature fields obtained by (a) EX1 and (b) EX2 after more than three years integration. JANW produces three pairs of alternating warm and cold regions along the eastern coast (Fig.27a). They are induced by the local wind stress curl fields caused by three strong, jet-like northerly winds (Figs 8, 9). The warm gyres off the Gulfs of Tehuantepec and Papagayo move westward or southwestward, and, after a few months, new gyres are induced in the same area. These are the same phenomena described in section 3. In this experiment, the cold region corresponding to the Costa Rica Dome has features different from those in the results of EX0 (Fig.13). The cold maximum at a place corresponding to the Costa Rica Dome in May is relatively stable. However, the other two cold maxima in the southwestern part vary their strength periodically. The northern

sides meander in connection with westward propagating warm gyres.

The results of EX2, a fixed MAYW experiment, are shown in Fig.27b. MAYW makes a zonally elongated cold region along 10° N latitude, between the southern NECC and the northern NEC. It is stable and has just the feature as the eastern end of the tropical current systems suggested by Wyrtki(1964). The location of the cold maximum is about 1000 km west of the cyclonic curl maximum of the wind stress (Fig.9). These results show MAYW, the typical southerly winds, causing strong zonal currents and then make a large stable cold region not related to the wind stress curl. However, it is not enough to form the dome-like cold region as in the mature stage of the Costa Rica Dome. Cane (1979) and Philander and Pacanowski (1981) also show the formation of the countercurrent caused by southerly winds blowing from the southern hemisphere over the equator.

Figure 28a shows the results of EX3 in which the wind is JANW as switched from MMW in January of the fourth year. The January temperature fields are the same as those of EX0 in January (Fig.13). In May, a clear cold region is found at the place where the May Costa Rica Dome is found in EX0. In September, the temperature fields are modified but basic features are not changed from those of May.

Figure 28b shows the results of EX4. The monthly mean varying winds drive the model after three years forcing by JANW. The results of May and September are the same as those of EX0 except for the meandering at the northern side of the cold region

(Fig.13). The results suggest that the features of the cold region, in particular its shape, depend on past features, at least on the order of one year.

Figure 29a shows the results of EX5. The fixed MAYW, switched in May after over three years forcing by MMW, drives the model continuously. The temperature fields in May of the fourth year are the same as those of EX0. This experiment well simulates the matured stage of the Costa Rica Dome in September. Though the temperature at the center is a little lower than that in EX0, the dome-like shape and its location are the same as those of EX0.

Figure 29b shows the results of EX6. The monthly mean winds, MMW, drive the model after being switched from the fixed MAYW. The results are the same as those of EX2 in which the winds are fixed MAYW. These experiments show the southerly winds producing a large cold area at about 10°N where the Costa Rica Dome is found in its matured stage. However, another condition, the formation of a small, but clear dome-like cold region in late spring or early summer off Central America, is necessary for generating a dome-like cold area in September, like sowing the seed of the Dome.

Previous experiments show that the northerly and southerly winds are important in the development of the Costa Rica Dome. Therefore, an experiment driven by either one of these two winds, JANW and MAYW is carried out. The experiment EX7 shows that they are basically responsible for the annual march of the Costa Rica Dome. The results shown in Fig.30 are similar to those of EX0 which was forced by monthly varying winds. The Costa Rica Dome

initial stage in May, the mature stage in September, and the decay stage in January when the seed of the Costa Rica Dome is being generated, are well simulated as shown in EX0. The features in January differ slightly from those of Fig.13. This is because the northerly wind starts blowing in October or November in EX0. The annual evolution of the Costa Rica Dome is basically well simulated by using only January and May winds.

### 6.3 Summary of Section 6

In order to understand the role of wind in the generation and maintenance mechanisms of the Costa Rica Dome, numerical experiments are carried out using a fine horizontal resolution regional model. The model is the same as that used in section 3 except for the forcing winds. The results of the experiments are compared to those of the model driven by climatological monthly mean wind fields. In the eastern tropical Pacific ocean off central America two kinds of winds are typical. In winter, three strong jet-like northers winds passing through three passes in Central America blow from the Atlantic to the Pacific ocean. From early summer to fall, southerly winds blow into the ITCZ with its northward migration. In this section it is shown that these winds play important roles in the generation and maintenance of the Costa Rica Dome.

The southerly winds in May cause the NECC and NEC, and then make a large stable cold region unrelated to the wind stress curl (Figs 9, 27b). However, they are not enough to form the dome-like cold region of the Costa Rica Dome major stage (compare to Fig.13).

The cold maximum is located about 1000 km west of the cyclonic curl maximum of the wind stress. In contrast, the northerly winds in January make three pairs of warm and cold regions along the eastern coast, locations related exactly to the wind stress curl (Fig.9, 27a). The cold region off the Gulf of Papagayo is formed in the same region with EX0 in May, and has a dome-like shape. However, the wind is not enough to cause the evolution of the large Costa Rica Dome mature stage (Figs 27a, 28a).

In experiments EX4 and EX5, the Costa Rica Dome's mature stage is accomplished in September (Fig.28b, 29a). In both cases, relatively small dome-like cold regions exist in May off the Gulf of Papagayo (see Fig.13 for EX5). After forming the cold region, southerly winds force the model ocean. Considering the results of EX2 and Ex3 (see Figs 27b, 28a), this shows that the northerly and southerly winds play important and different roles. The former is responsible for the formation of the dome-like shape, and the latter is responsible for the expansion of the dome-like cold region. Both winds are necessary to accomplish the Costa Rica Dome's mature stage.

The results of EX4 and EX5 show another interesting feature. The northern side of the Costa Rica Dome is remarkably meandering in EX4, but not in EX5 or in the results of section 3 (Fig.13). This is clearly due to the oceanic conditions from January or farther in the past. The features of the Costa Rica Dome, in particular its shape, are considerably affected by past features at least on the order of one year. This is probably one of the

reasons why it has been difficult to obtain a coherent picture of the observed Costa Rica Dome.

## 7. Summary and concluding remarks

In order to obtain a coherent picture of how the oceanic conditions vary in the eastern tropical Pacific ocean during a year, a regional ocean circulation model with a fine horizontal resolution of 0.25° x 0.25° has been developed. The model is initialized by use of the Levitus climatology of temperature field, and is forced by the Hellerman-Rosenstein monthly mean climatological winds with resolution of 1° x 1°. Several important conclusions useful for organizing past hypotheses and observations are obtained, and they are summarized as follows:

1. The model Costa Rica Dome with its center located near 10° N, 90° W, is generated in late spring off the Gulf of Papagayo, maturing in summer and early fall in accordance with the strengthening of the NECC due to the northward migration of the ITCZ. The diameter of the model Dome is about 300 - 500 km in summer, and the model Dome elongates in the zonal direction in fall as a long Rossby wave.

2. The cyclonic turn of the NECC, which is associated with subsurface water column stretching off the coast of Central America, is mainly responsible for the maintenance of the model Costa Rica Dome in summer and fall. This is consistent with both the hypothesis of Wyrtki (1964) and the hydrographic observations of Barberan et al. (1985), but contradicts the hypothesis of

Hofmann et al. (1981).

3. In winter, strong northers converging to the southern-most ITCZ excite three noticeable warm anticyclonic gyres confined to the upper layer, each of which is accompanied by the comparatively weak cyclonic circulation. These model anticyclonic gyres are remarkably similar to those observed, and are expected to be real examples of the IG eddies as suggested by Matsuura and Yamagata (1982). The Costa Rica Dome is eroded by the warm gyres excited off the Gulf of Papagayo, and decays in winter and early spring.

4. The cyclonic circulations with strong upwelling in winter near the coast of Central America are generated by the local wind stress curl associated with the northers blowing to the Pacific ocean through the three passes in Central America. The northers are responsible for the complex ocean structure along the coast of Central America during winter and early spring. The cyclonic circulation that is excited off the Gulf of Papagayo acts as a seed for the Costa Rica Dome, which is clearly formed in late spring and early summer.

In this study a coherent picture of the eastern tropical Pacific ocean during a one year period is obtained. It is noteworthy in resolving the mystery of the Costa Rica Dome, that has been unclear for a long time. The hypothesis proposed by Wyrtki (1964) is more plausible than that proposed by Hofmann et al.

(1981). The Costa Rica Dome exists not only in summer but also in spring and fall. In particular, in summer the Dome is mainly maintained by the cyclonic turn of the NECC. However, it has to be emphasized that the Dome is not a steady phenomenon but is evolving during a year. These results are accomplished through the use of a numerical model having fine resolution and driven by fine resolution wind stress. The subsurface oceanic conditions are well simulated by the present model. However, it may be unsatisfactory in simulating the surface oceanic conditions. The improvement of the model will be continued in further investigations.

**Acknowledgements**

The author would like to express his sincere thanks to Dr. T. Yamagata for his stimulating guidance and encouragement throughout the course of this study, and to late Professor M. Uryu for his interest in the present study and encouragement. He also would like to thank Dr. K. Bryan and late M. Cox for permitting use of the GFDL OGCM and Mr. R. Pacanowski for his advice during the model adapting process.

He is very grateful to Drs S. Miyahara and H. Hukuda for their critical reading of the manuscript, and to Dr. C. Gordon and Mr. Y. Masumoto for informing him of their important unpublished works. Mr. V. Sullivan helped preparing the manuscript; his friendly help is highly appreciated.

The author is deeply indebted to his wife Akiko. Her understanding and encouragement made the work completed.

## References


Arakawa, A. and V. R. Lamb, 1977: Computational design of the basic dynamical processes of the UCLA general circulation model. Methods in Computational Physics, Vol.17,Academic Press, 174-265.

Barberan,J., A. Gallegos, A. Fernandez and L. Mee, 1985: Subsurface origin of the Costa Rica Dome. Unpublished manuscript.

Broenkow, W., 1965: The distribution of nutrients in the Costa Rica Dome in the eastern tropical Pacific Ocean. Limnol. Oceanogr., **10**, 40-52.

Bryan, K. and M. D. Cox, 1967: A numerical investigation of the oceanic general circulation. Tellus, **19**, 54-80.

Bryan, K., 1969: A numerical method for the study of the world ocean. J. Comput. Phys., **4**,347-376.

Bryan, K. and M. D. Cox, 1972: An approximate equation of state for numerical models of ocean circulation. J. Phys. Oceanogr., **2**,510-514.

Busalacchi, A.J. and J. J. O'Brien, 1980: The Seasonal Variability in a Model of the Tropical Pacific. J. Phys. Oceanogr., **10**, 1929-1951.

Cane, M. A., 1979: The response of an equatorial ocean to simple windstress patterns. J. Mar. Res., **37**, 253-299.

Charney, J. G. and G. R. Flierl, 1981: Oceanic analogues of large-scale atmospheric motions. Evolution of Physical Oceanography (the Stommel volume). B. A. Warren and C. Wunsch, Eds., MIT Press, 504-548.

Clarke, A. J., 1988: Inertial wind path and sea surface temperature patterns near the Gulf of Tehuantepec and Gulf of Papagayo. J. Geophys. Res., **93**, 15491-15501.

Cox, M. D., 1984: A primitive equation, 3-dimensional model of the ocean. GFDL Ocean Group Tech. Rep. No.1, 143 pp.

Cromwell,T.,1958: Thermocline topography, horizontal currents and "ridging" in the eastern tropical Pacific. Inter.-Am. Trop. Tuna Comm. Bull., **3**, 135-164.

Goldenberg, S.O. and J.J. O'Brien, 1981: Time and space variability of tropical Pacific wind stress. Mon. Wea. Rev., **109**, 1190-1207.

Haney, R. L., 1971; Surface thermal boundary conditions for ocean circulation model. J. Phys. Oceanogr., **1**, 241-248.

Hellerman, S. and M. Rosenstein, 1983: Normal monthly wind stress over the world ocean with error estimates. J. Phys. Oceanogr., **13**, 1093-1104.

Hofmann, E. E., A. J. Busalacchi and J. J. O'Brien, 1981: Wind generation of the Costa Rica Dome. Science, **214**, 552-554.

Hurd, W. E., 1929: Northers of the Gulf of Tehuantepec. Mon. Wea. Rev., **57**, 192-194.

Jones, J. H., 1973: Vertical mixing in the Equatorial Undercurrent. J. Phys. Oceanogr. **3**, 286-296.

Knauss, J. A., 1978: Introduction to Physical Oceanography, Prentice-Hall, Inc., New Jersey, 338 pp.

Leetmaa, A., 1982: Observations of near-equatorial flows in the eastern Pacific. J. Mar. Res., **40** (Supplement), 357-370.

Legeckis, R., 1988: Upwelling off the Gulfs of Panama and Papagayo in the tropical Pacific during march 1985. J. Geophys. Res., **93**, 15485-15489.

Levitus, S., 1982: Climatological Atlas of the World Ocean. NOAA Prof. Paper **13**, 173pp., 17 microfiche, U.S. Govt. Printing Office, Washington, D. C.

Matsuura, T. and T. Yamagata, 1982: On the evolution of nonlinear planetary eddies larger than the radius of deformation. J. Phys. Oceanogr., **12**, 440-456.

McCreary, J. P., H. S. Lee and D. B. Enfield, 1988: The response of the coastal ocean to strong offshore winds: with application to circulations in the Gulfs of Tehuantepec and Papagayo. J. Mar. Res., **47**, 81-109.

Pacanowski, R. and S. G. H. Philander, 1981: Parameterization of vertical mixing in numerical models of tropical oceans. J. Phys. Oceanogr., **11**, 1443-1451.

Pedlosky, J., 1979: Geophysical Fluid Dynamics, 1st edition, Springer-Verlag, Berlin, 624pp.

Philander, S. G. H. and R. Pacanowski, 1981: The oceanic response to cross-equatorial winds (with application to coastal upwelling in low latitudes). Tellus, **33**, 201-210.

Philander, S. G. H., 1983: El Niño Southern Oscillation phenomena. Nature, **302**, 295-301.

Philander, S. G. H., W. J. Hurlin and A. D. Seigel, 1987: Simulation of the seasonal cycle of the tropical Pacific Ocean. J. Phys. Oceanogr., **17**, 1986-2002.

Philander, S.G.H., D. Halpern, D. Hansen, R. Legeckis, L. Miller, C. Paul, R. Watts, R. Weisgerg and M. Wimbush, 1985: Long waves in the equatorial Pacific Ocean. Eos Trans. AGU, 66(14), 154.

Philander, S. G. H. and A. D. Seigel, 1985: Simulation of El Nino of 1982-1983. Coupled Ocean-Atmosphere Models. J. Nihoul, Ed., Elsevier, 517-541.

Reed, R. K., 1983: Heat fluxes over the eastern tropical Pacific and aspects of the 1972 El Nino. J. Geophys. Res., **88**, 9627-9638.

Reed, R. K., 1985: An estimate of the climatological heat fluxes over the tropical Pacific Ocean. J. Climate Appl. Meteor., **24**, 833-840.

Robinson, A. R., 1966: An investigation into the wind as the cause of the Equatorial Undercurrent. J. Mar. Res. **24**,179-204.

Roden, G. I., 1961: On the wind driven circulation in the Gulf of Tehuantepec and its effect upon surface temperatures. Geofis. Int., **1**: 55-72.

Rosati, A. and K. Miyakoda, 1988: A General Circulation Model for Upper Ocean Simulation. J. Phys. Oceanogr., **18**, 1601-1626.

Stumpf, H. G., 1975: Satellite detection of upwelling in the Gulf of Tehuantepec, Mexico. J. Phys. Oceanogr., **5**, 383-388.

Stumpf, H. G. and R. V. Legeckis, 1977: Satellite observations of mesoscale eddy dynamics in the eastern tropical Pacific Ocean. J. Phys. Oceanogr., **7**, 648-658.

Thomas, W. H., 1979: Anomalous nutrient-chlorophyll interrelationships in the offshore eastern tropical Pacific Ocean. J. Mar. Res., **37**, 327- 335.

Williams, G. P. and T. Yamagata, 1985: Geostrophic regimes, intermediate solitary vortices and Jovian eddies. J. Atmos. Sci., **41**, 453-478.

Wyrtki, K., 1964: Upwelling in the Costa Rica Dome. Fish. Bull., **63**, 355-372.

Wyrtki, K., 1967: Circulation and Water Masses in the Eastern Equatorial Pacific Ocean. Int. J. Oceanol. & Limnol., **1**, 117-147.

Wyrtki, K., 1974: Equatorial Currents in the Pacific 1950 to 1970 and Their Relations to the Trade Winds. J. Phys. Oceanogr., **4**, 372-380.

Yamagata, T., 1982: On nonlinear planetary waves: a class of solutions missed by the quasi-geostrophic approximation. J. Oceanogr. Soc. Japan, **38**, 236-244.

Yamagata, T., 1986: On the Recent Development of Simple, Coupled Ocean-Atmosphere Models of ENSO. J. Oceanogr. Soc. Japan, **42**, 299-307.

Table 1. Horizontal grid resolution and wind stress resolution (longitude x latitude) used in the present model and two global models (G1 and G2).

| MODEL | GRID RESOLUTION | WIND RESOLUTION |
|---|---|---|
| Present model | 0.25° x 0.25° | 1° x 1° |
| G1 | 0.5° x 0.5° | 1° x 1° |
| G2 | 0.5° x 0.33° | 2° x 2° |

Table 2. Types of the wind forcing used in the EX1 - EX7. The JANW, MAYW and MMW correspond to climatologically averaged January, May and monthly winds, respectively. Jan., May and Dec. refer to the months in the fourth year.

| EXPERIMENT | WIND FORCING (fourth year) Jan. May Dec. |
|---|---|
| EX1 | ——————— JANW ———————————> |
| EX2 | ——————— MAYW ———————————> |
| EX3 | – MMW —>\|———————— JANW ———————> |
| EX4 | – JANW –>\|———————— MMW ———————> |
| EX5 | – MMW ———————>\|——— MAYW ————> |
| EX6 | – MAYW ———————>\|——— MMW ————> |
| EX7 | – – – – >\|– JANW –>\|—— MAYW —>\|– – –> |

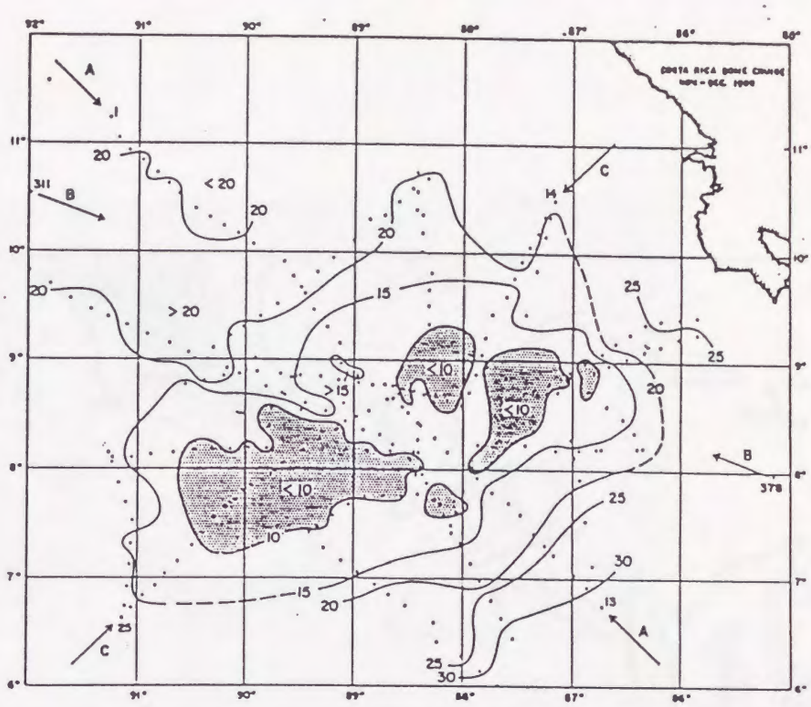


Figure 1: Topography of the 24° C isotherm in meters, during November and December 1959. The depth less than 10 m is shaded (after Wyrtki, 1964).

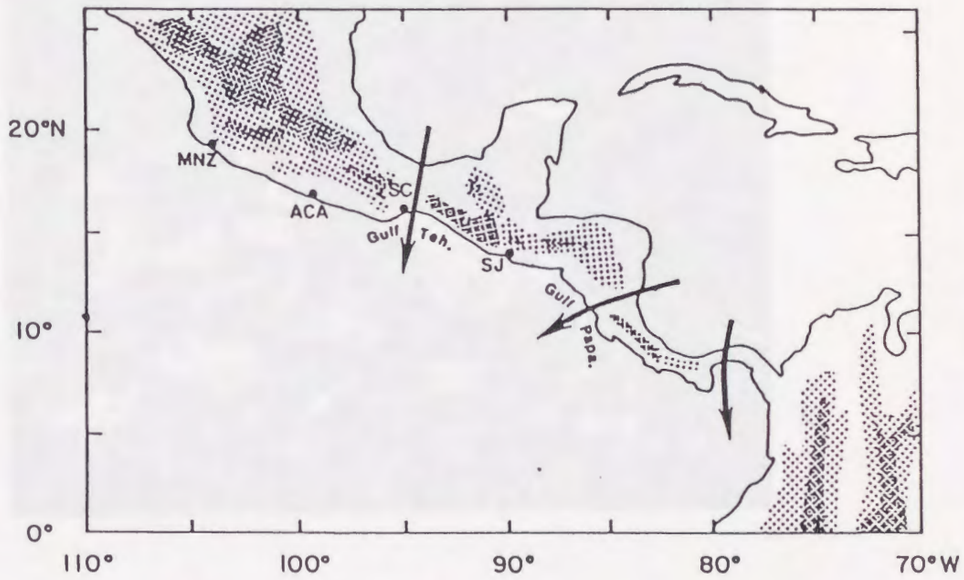


Figure 2: A map showing the locations of the three mountain-pass jets. Light and dark shaded regions indicate the places where the elevation of the topography is greater than 650 and 2000 m, respectively (after McCreary et al., 1989).


Figure 3: Satellite SST image for the Central American region on 29 January, 1986 (after Clarke, 1988). Warm gyres and cold upwelling regions are generated by wind passing through mountainpasses.

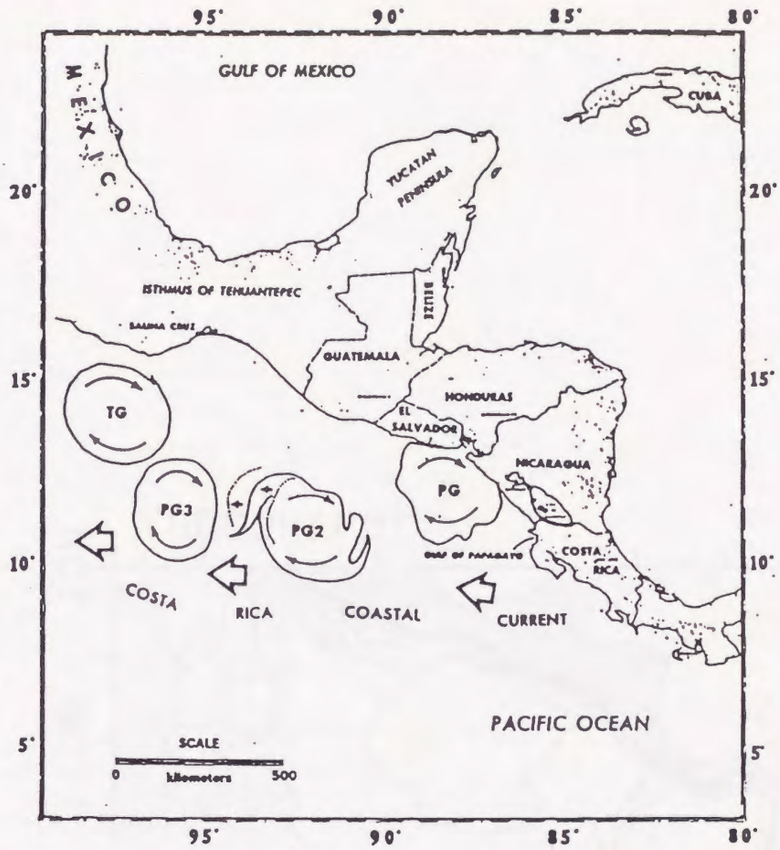


Figure 4: Composite diagram showing the coherent anticyclonic gyres observed during February 1979 (after Stump and Legeckis, 1977).

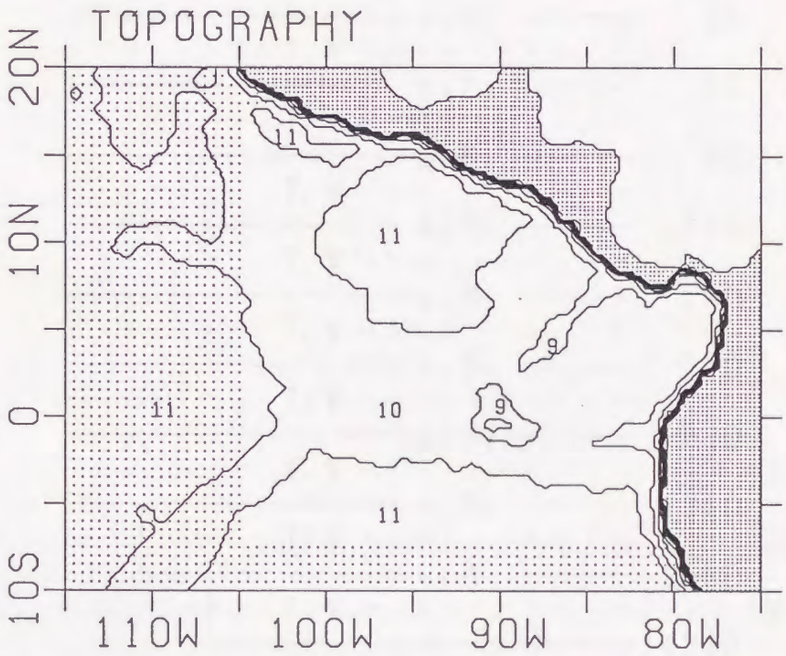


Figure 5: Coastlines and bottom topography of the regional model. Light shaded regions are high viscous buffer layer. The numbers indicate the number of the vertical levels.

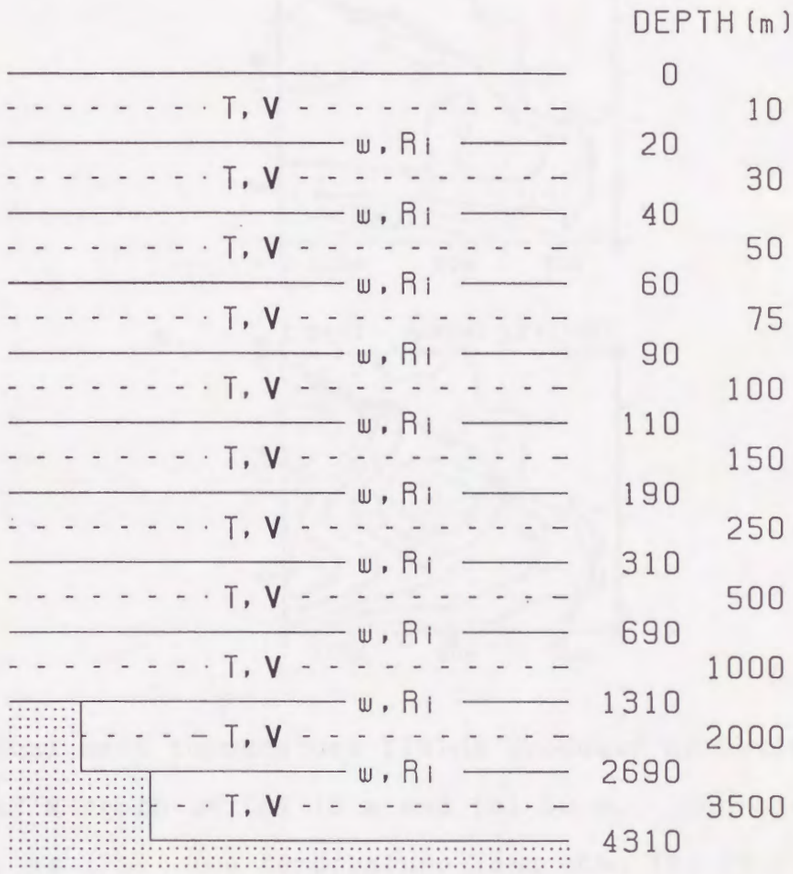


Figure 6: A schematic diagram of the vertical resolutions with the placement of the variables.

a.

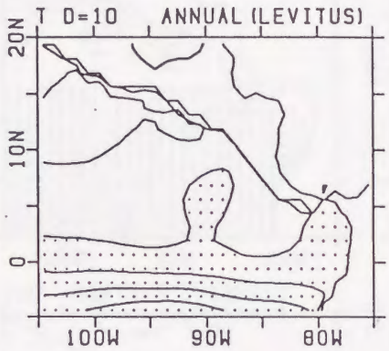


b.

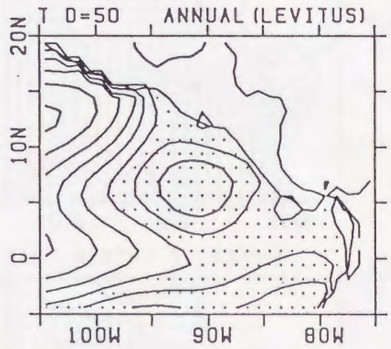


Figure 7: Annual mean temperature fields produced by Levitus (1982) at a depth of (a) 10 m and (b) 50 m. Contour interval is 1°C. The temperature less than (a) 27°C, and (b) 20°C is shaded.

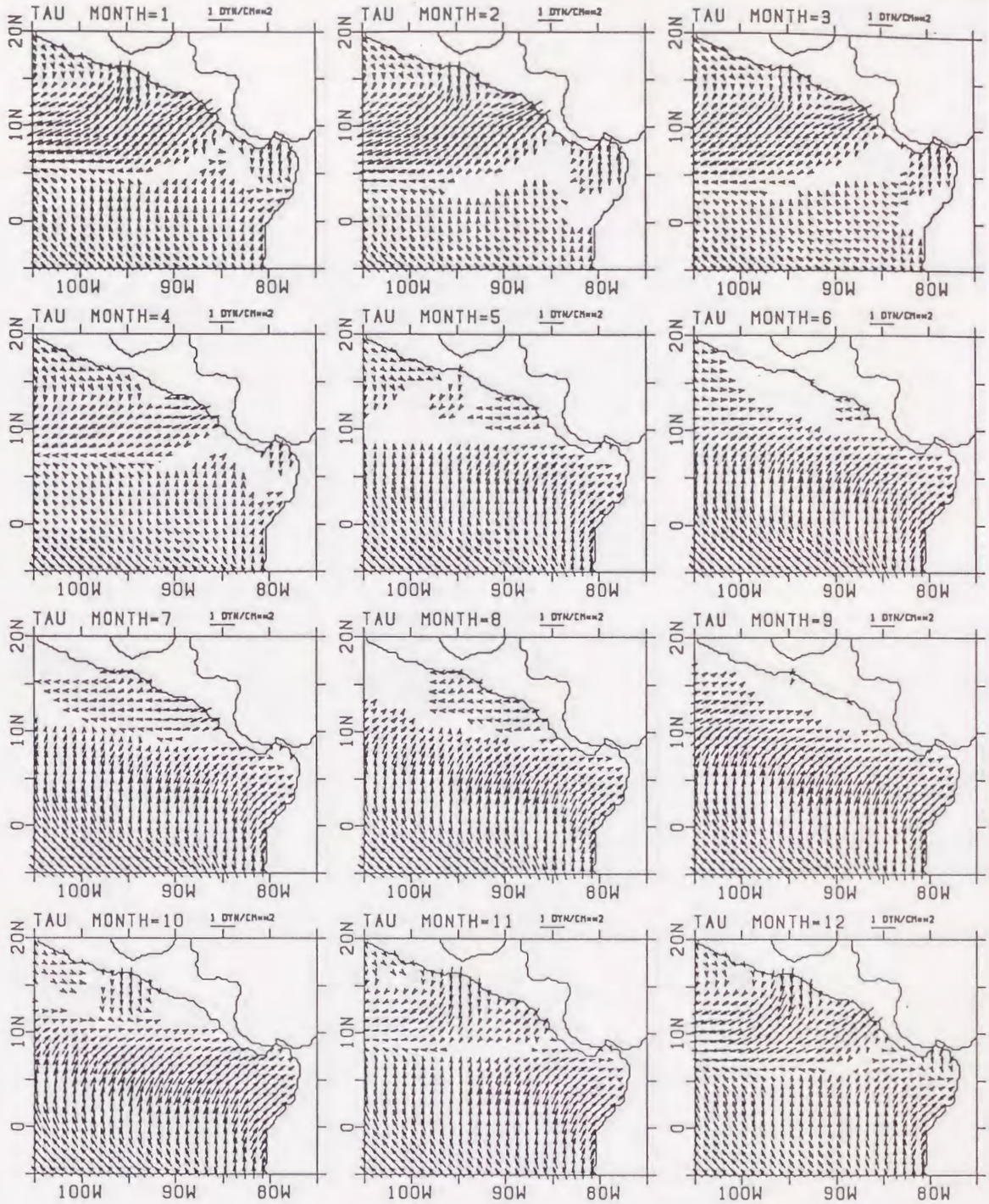


Figure 8: Hellerman-Rosenstein monthly mean wind stresses used in the present work. The three winter northers through three passes in Central America are well resolved.

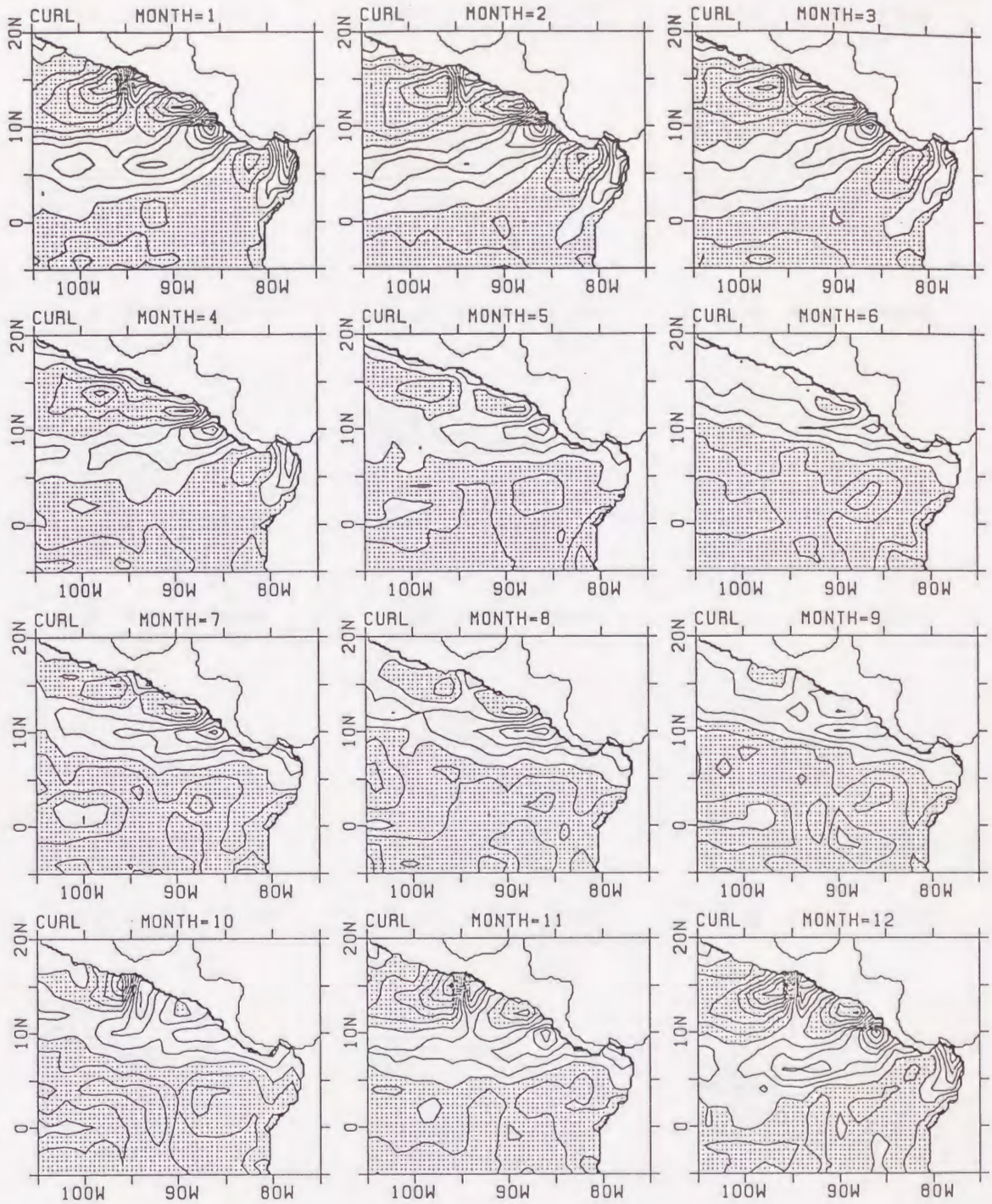


Figure 9: Curl of the Hellerman-Rosenstein wind stresses. Contour interval is 5 x $10^{-9}$ dyn $cm^{-3}$. The negative valued area is shaded.

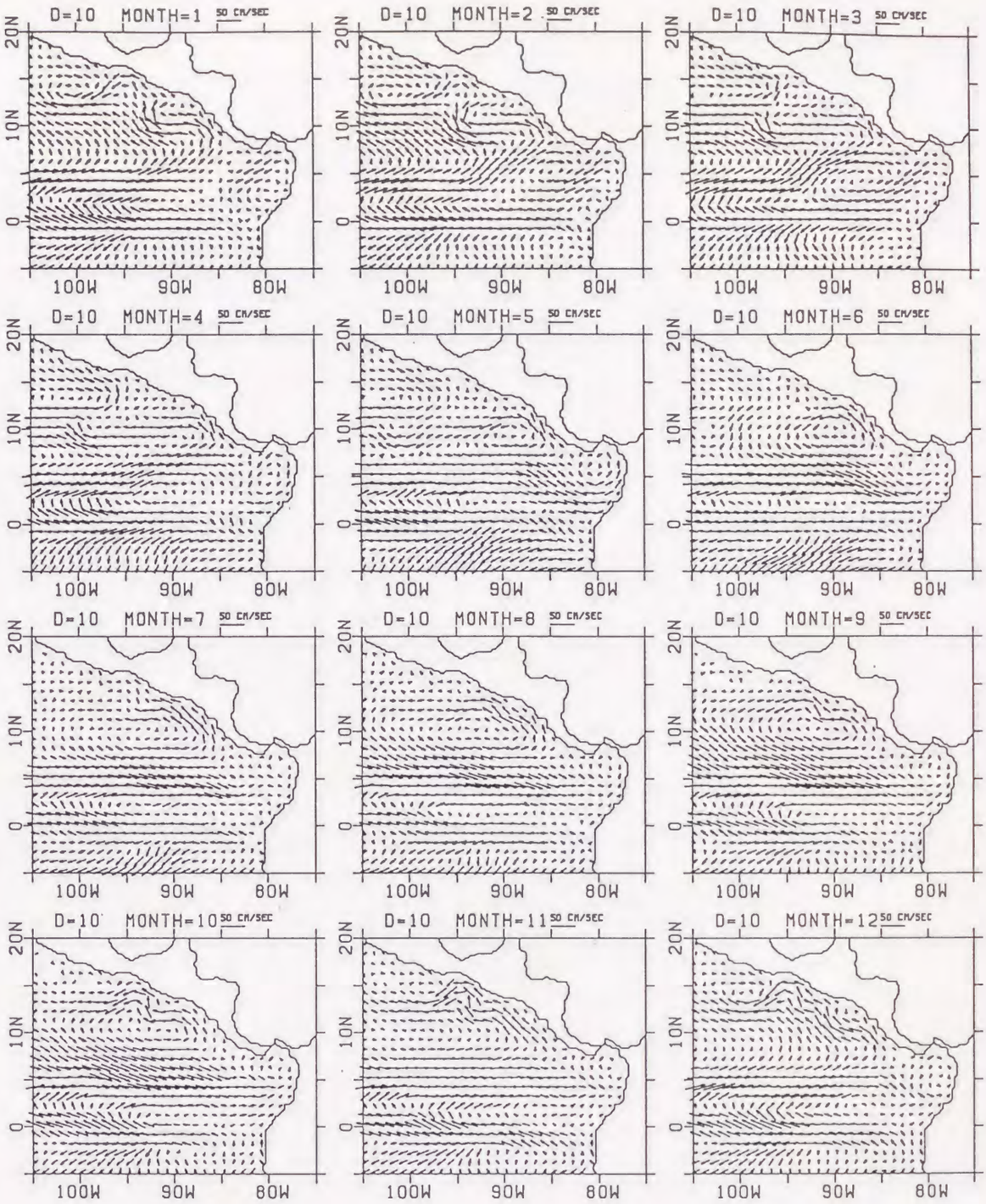


Figure 10: Annual march of horizontal velocity vectors at a depth of 10 m.

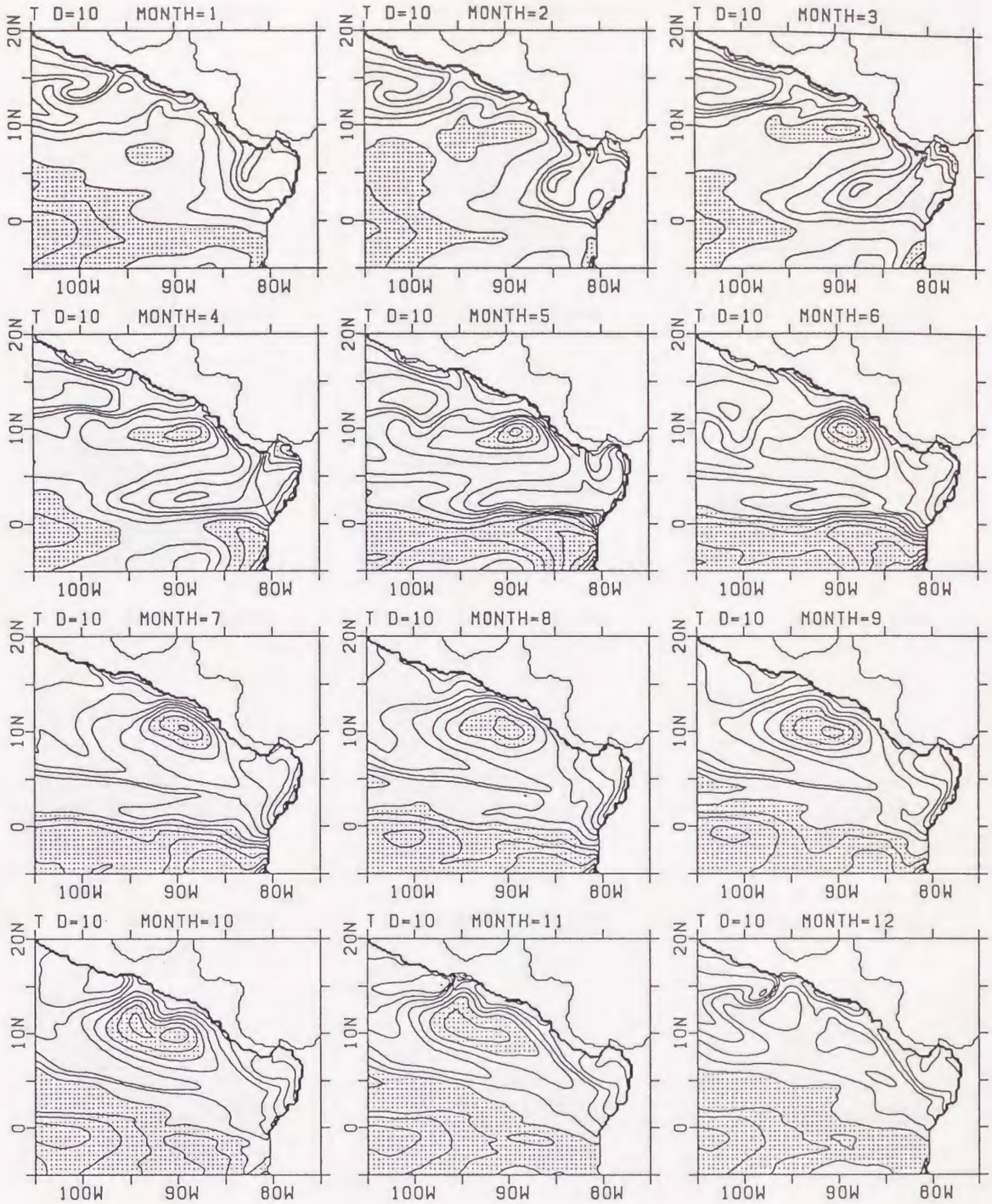


Figure 11: Annual march of surface temperatures at a depth of 10 m. Contour interval is 1°C. The temperature less than 28°C is shaded.

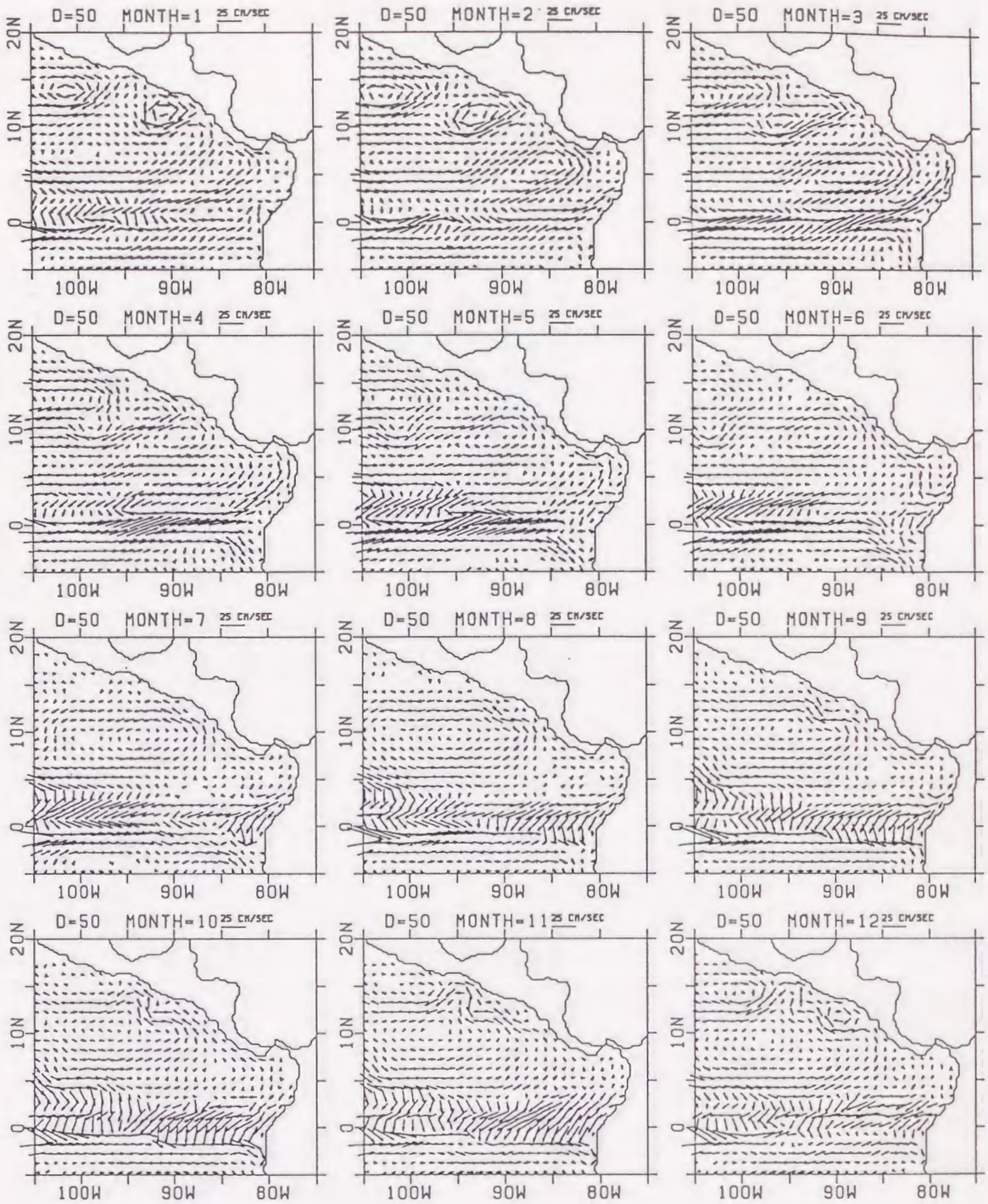


Figure 12: Annual march of horizontal velocity vectors at a depth of 50 m.

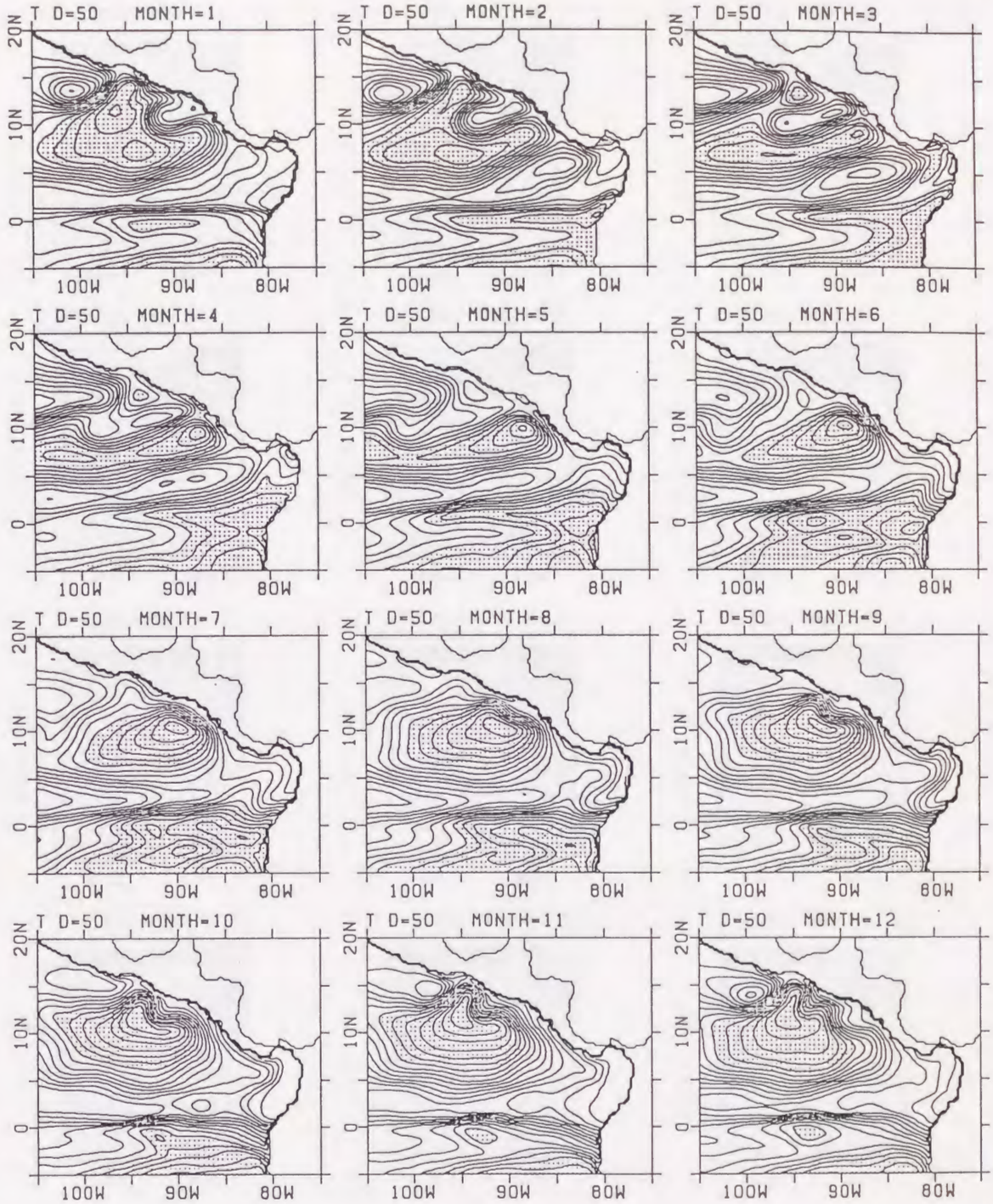


Figure 13: Annual march of subsurface temperatures at a depth of 50 m. Contour interval is 1°C. The temperature less than 20°C is shaded.

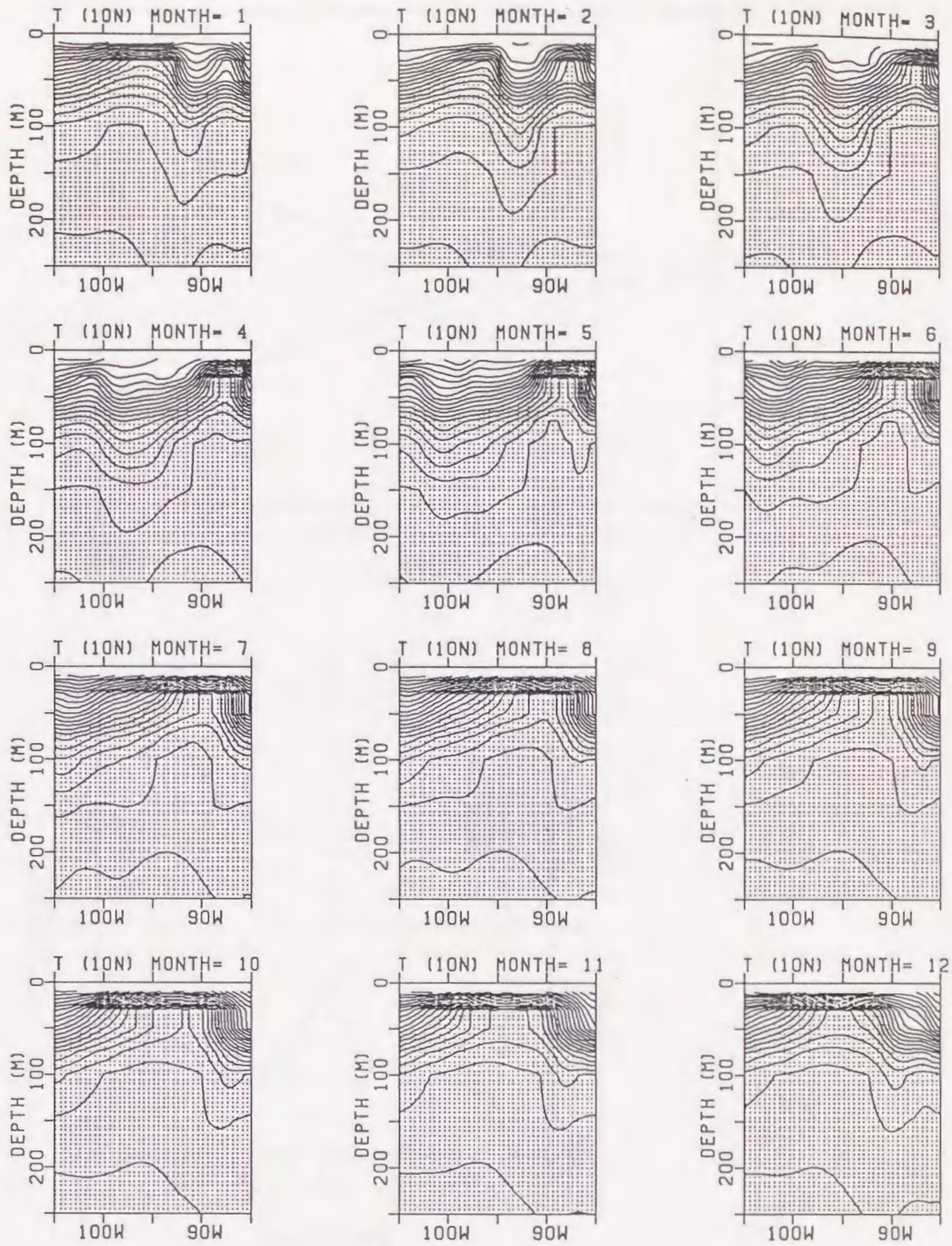


Figure 14: Annual march of zonal section of temperature along 10° N. Contour interval is 1° C. The temperature less than 20° C is shaded.

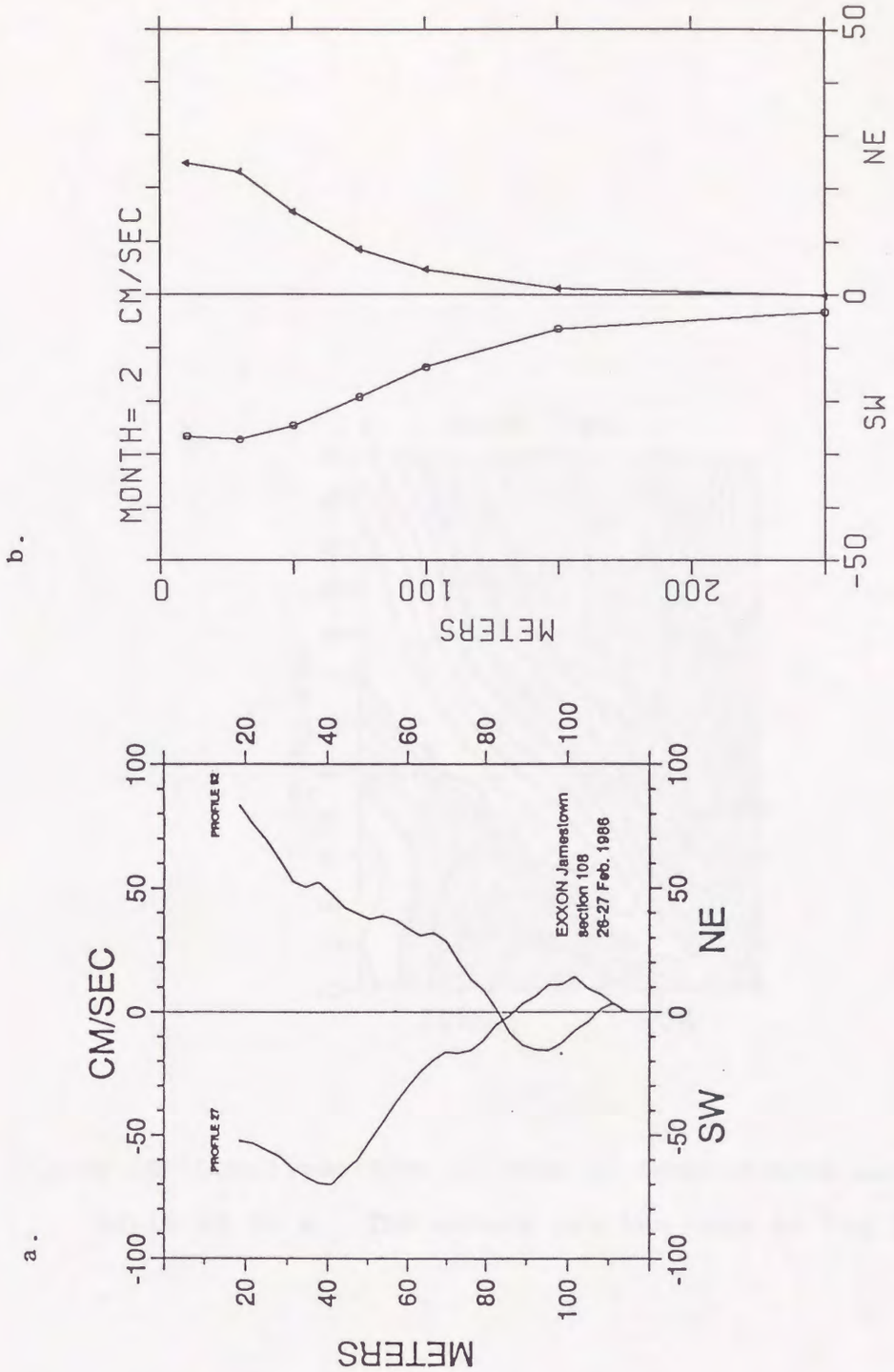


Figure 15: Velocity profiles near the current maxima on either side of anticyclonic gyres off the Gulf of Papagayo. The gyres were (a) observed on February 27, 1986, by means of an Acoustic Doppler Current Profiler (ADCP), and (b) simulated in the present model on February 15. The locations of their center are (a) 10.5° N, 92° W, and (b) 11° N, 92.5° W.

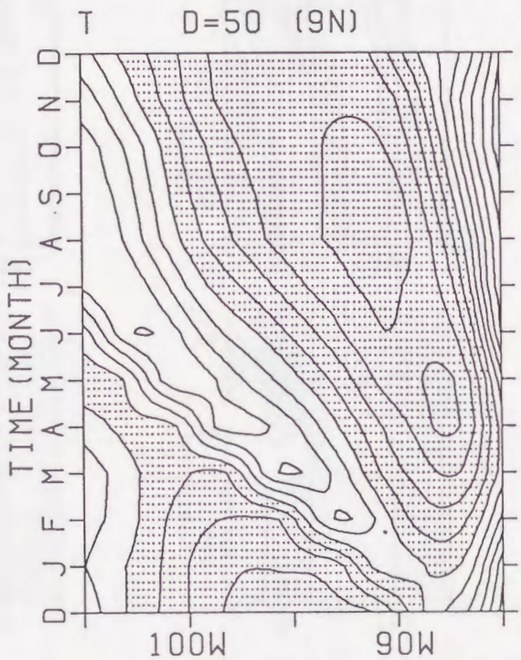


Figure 16: Longitude-time section of temperatures along 9°N at a depth of 50 m. The others are the same as Fig.13.

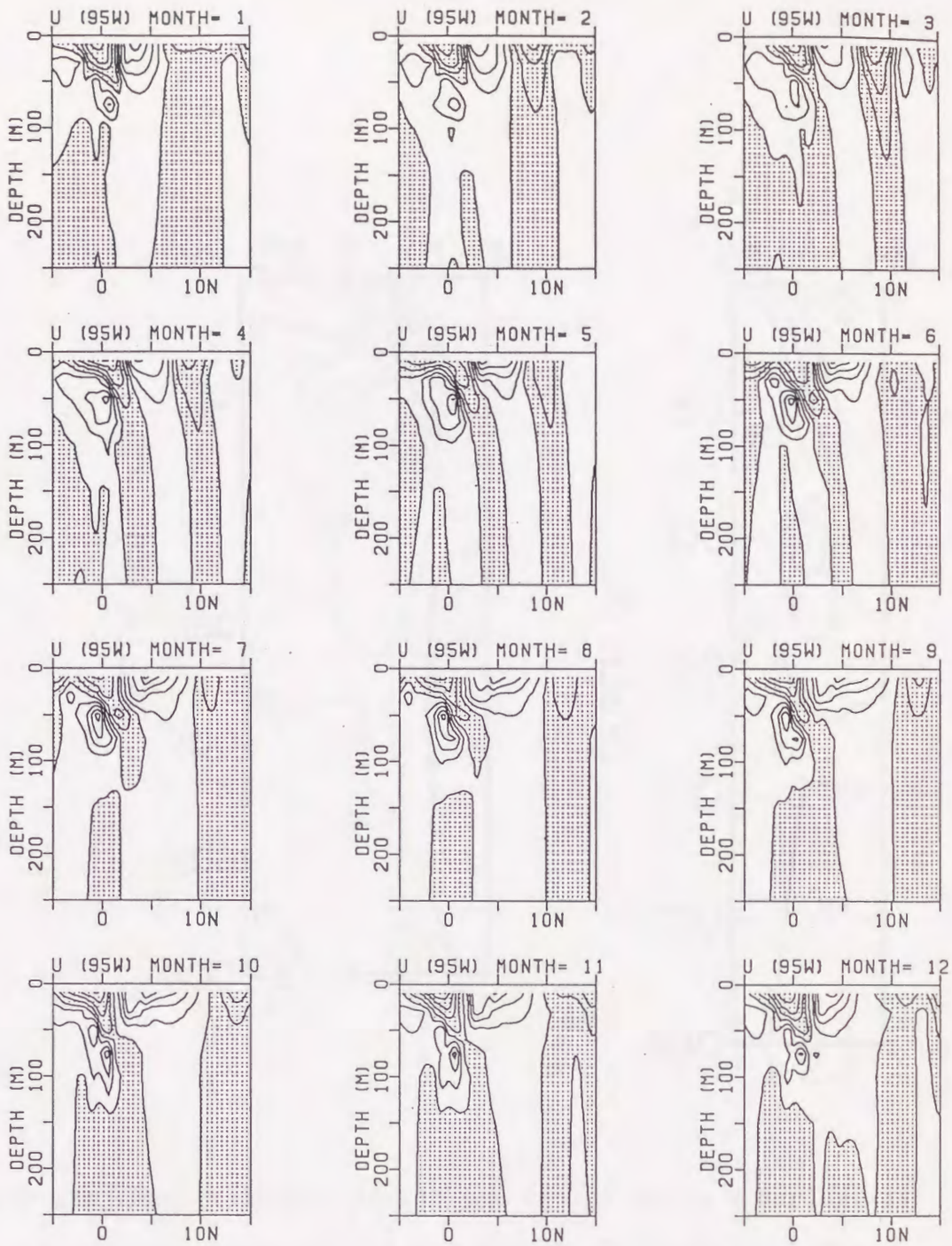


Figure 17: Annual march of meridional sections of zonal velocity along 95° W. Contour interval is 10 cm $sec^{-1}$. Shaded areas indicate westward flow.

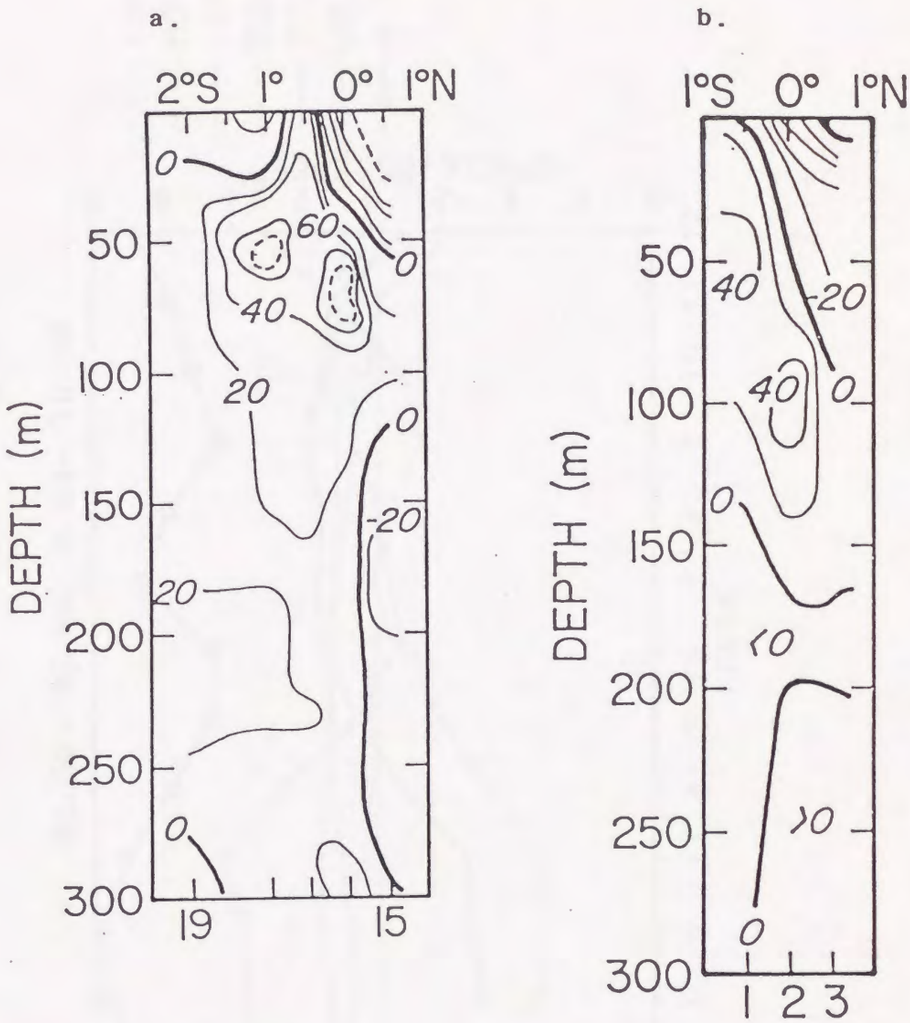


Figure 18: Zonal velocity fields (cm $sec^{-1}$) at 95° W during (a) 11-15 June, 1981 and (b) 2-5 August, 1980 (after Leetmaa, 1982).

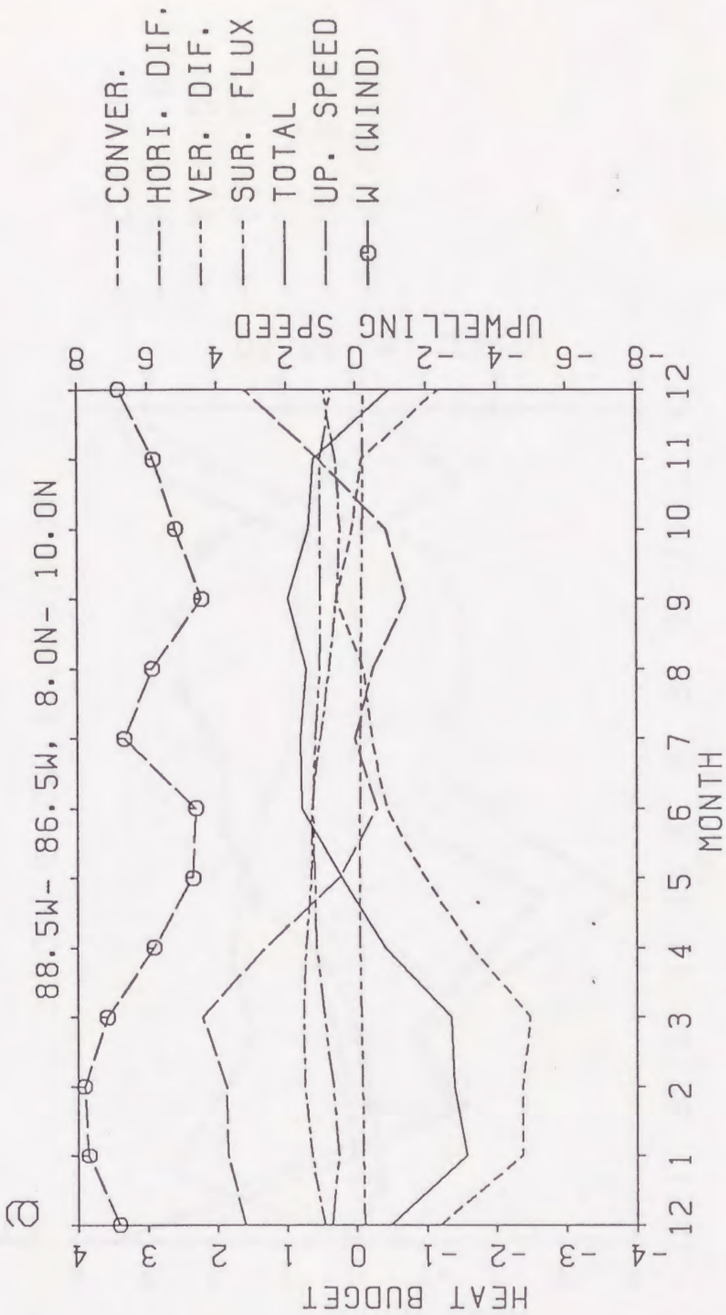


Figure 19a: Monthly mean values of the heat budget for box A (in $10^{12}$ cal/sec). The rate of change of heat storage is governed by the convergence of heat transport ( ---- ), flux across the surface ( —-- ), horizontal ( —-- ) and vertical ( —---- ) diffusion. The upwelling speed ($10^{-4}$ cm/sec; —— ) at a depth of 60 m and the wind induced upward velocity($10^{-4}$ cm/sec; —⊖— ) estimated by Ekman's theory are also shown.

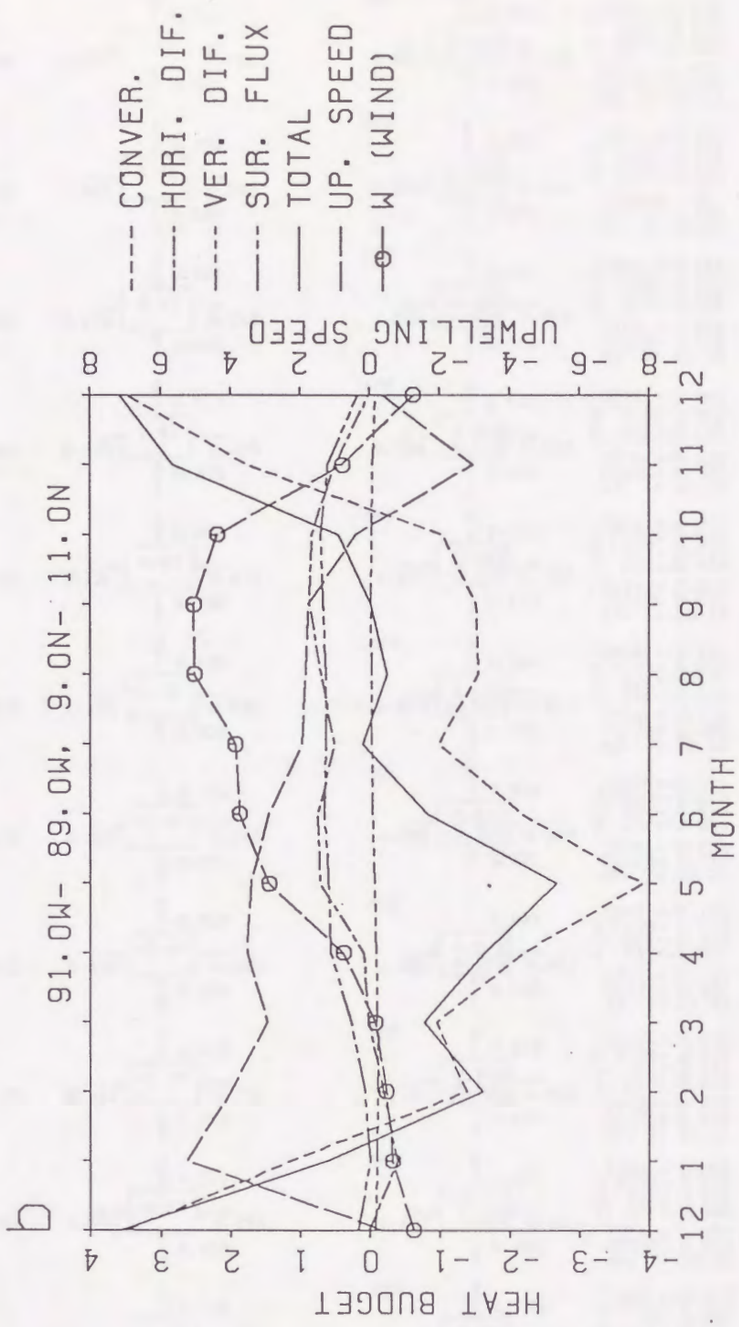


Figure 19b: Same as in Fig.19a but for box B.

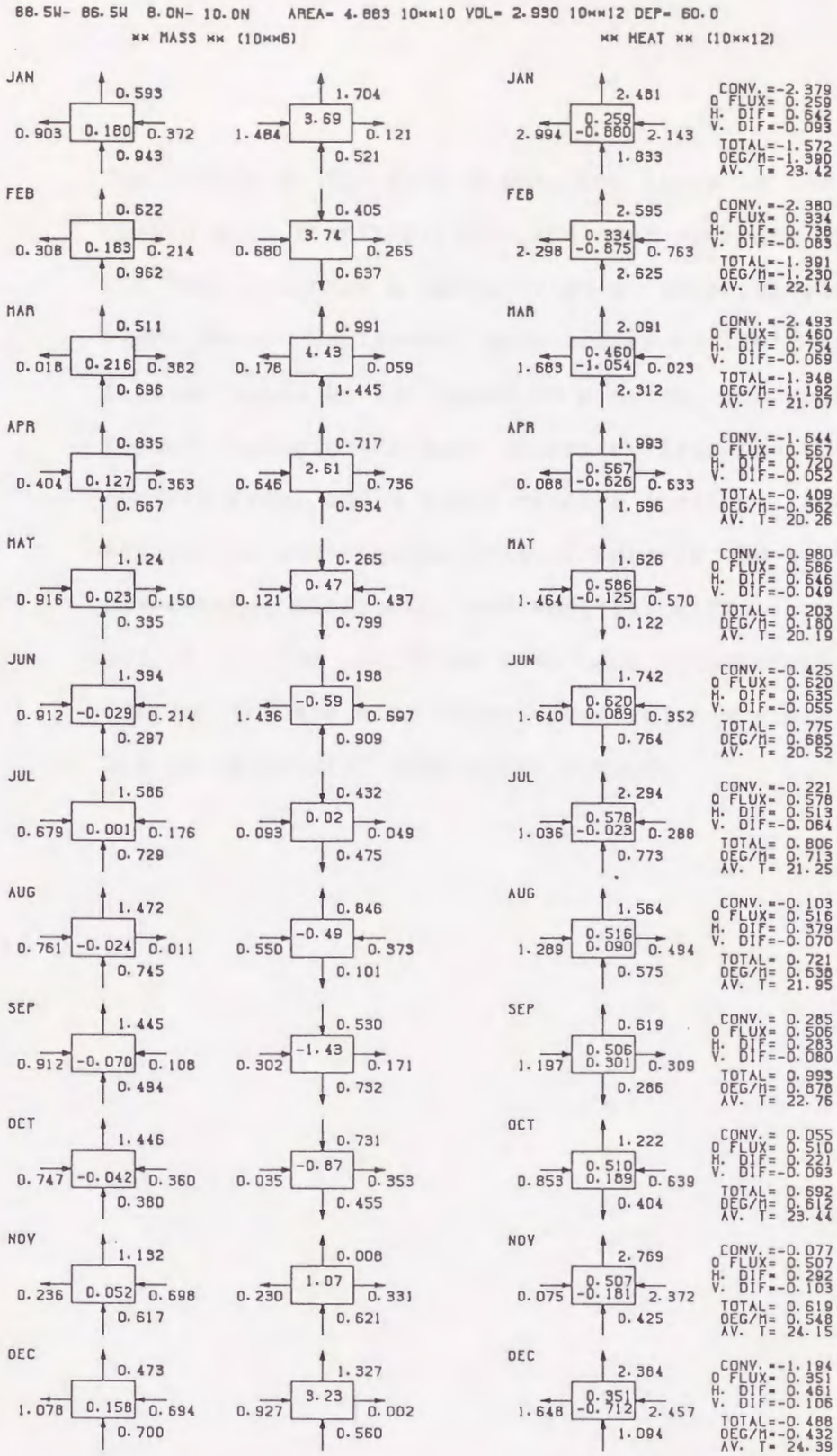


Figure 20a: Mass and heat transport across the walls of box A: Horizontal mass transport (Sv = $10^6 m^3$/sec) across lateral walls in the upper layer above 60 m (left panel) and the lower layer below 60 m (middle panel). (continued)

The values in the left frames and those in the middle are upward mass transport (Sv) and area-averaged upwelling speed ($10^{-4}$cm/s) across a depth of 60 m, respectively.
Right panel: Horizontal heat transport ($10^{12}$ cal/sec) across lateral walls in the upper 60 m depth. The values in the frames indicate the heat transport into the box across the surface (top) and a depth of 60 m (bottom). Heating of the box due to convergence (sum of lateral and vertical advection), horizontal and vertical diffusion, total heat budget and the estimated rate of a temperature change (deg/month) are also shown. Averaged temperature within the box is calculated from model results.

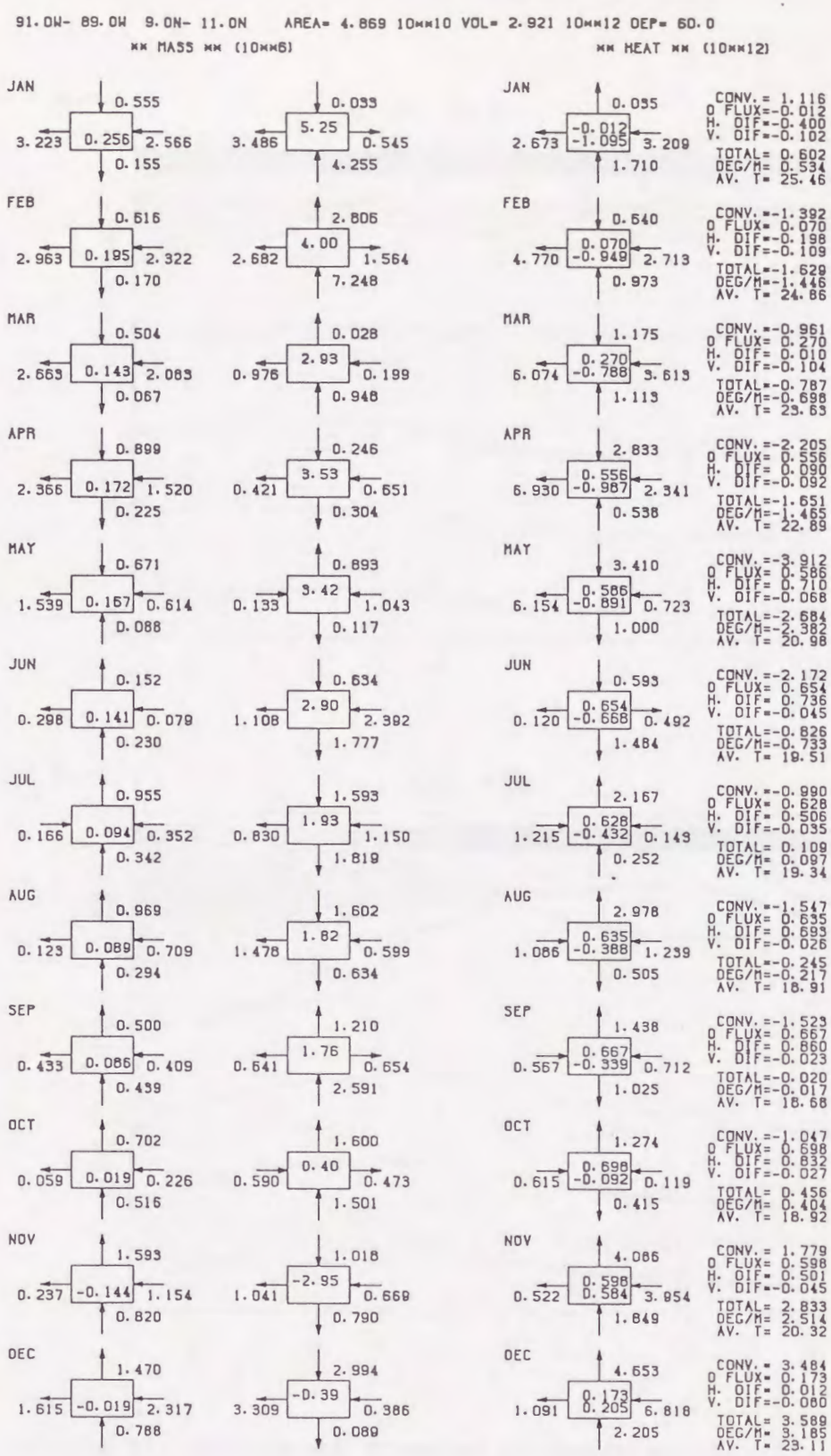


Figure 20b: Same as in Fig.20a except for box B.

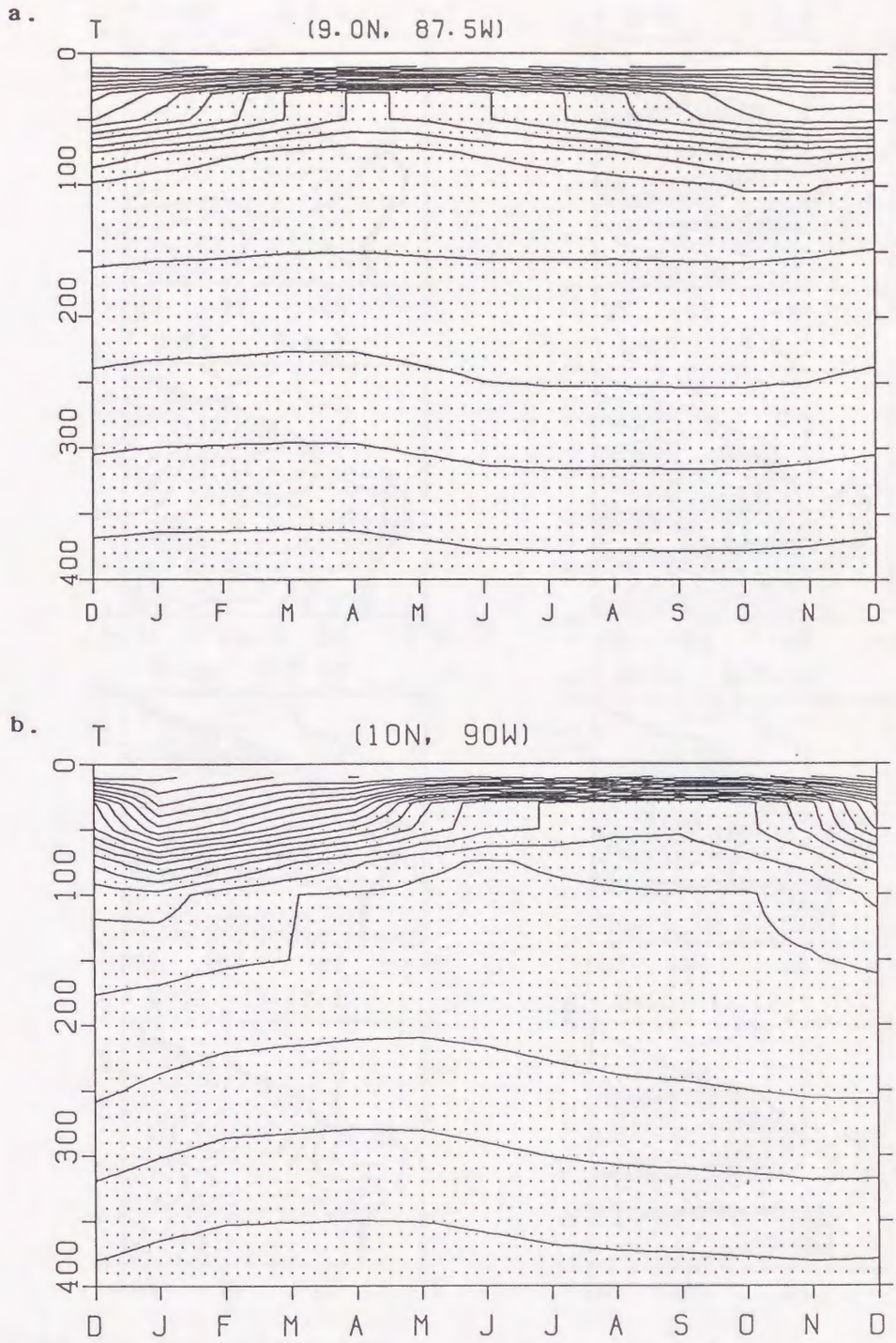


Figure 21: Time-depth diagrams of temperatures at a center of (a) box A and (b) box B.

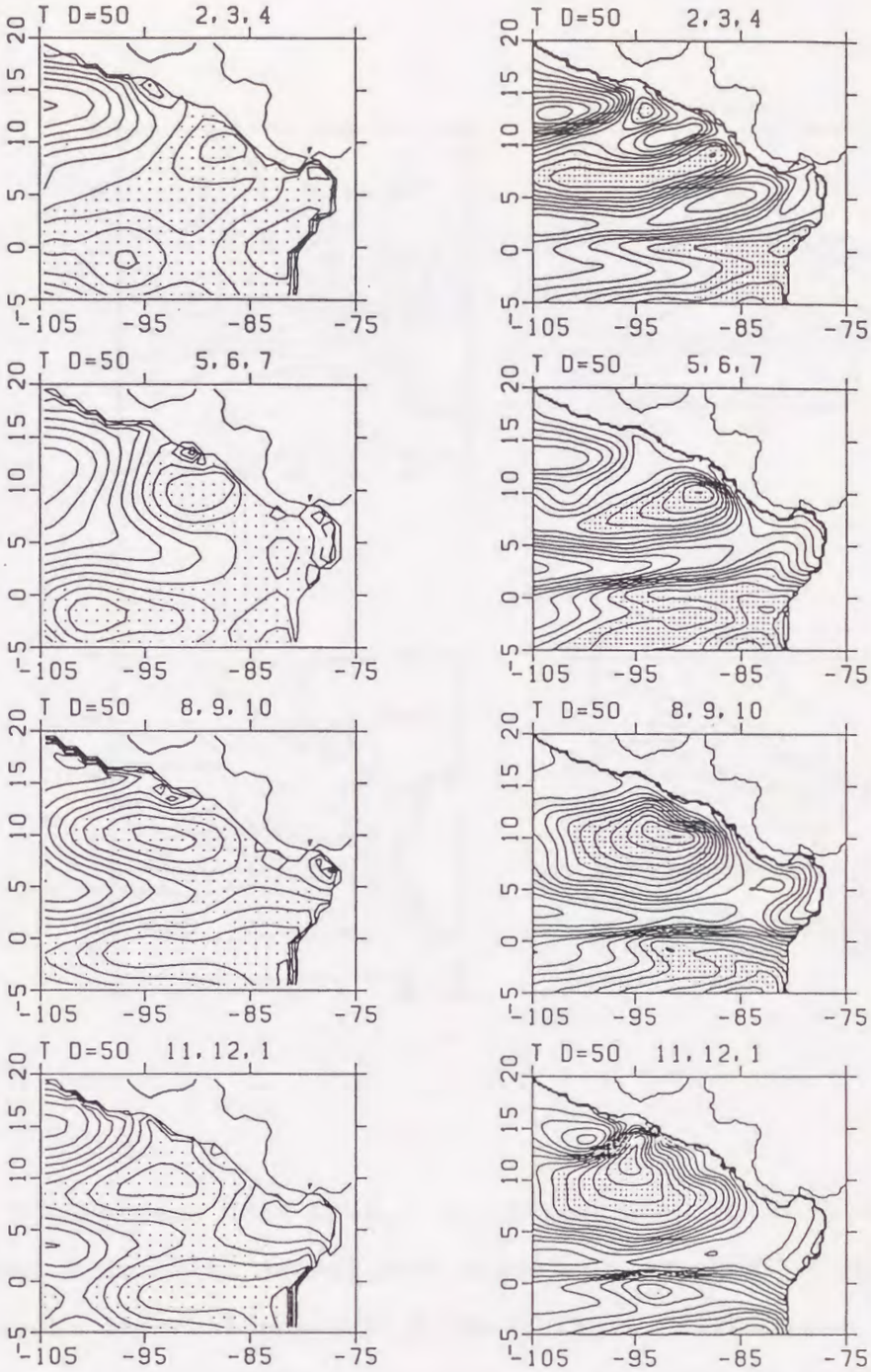


Figure 22: Subsurface temperatures averaged for three months at a depth of 50 m in four seasons. Left panel: Levitus climatology. Right panel: the present model simulation. Contour interval is 1°C. Temperatures less than 20°C are shaded.

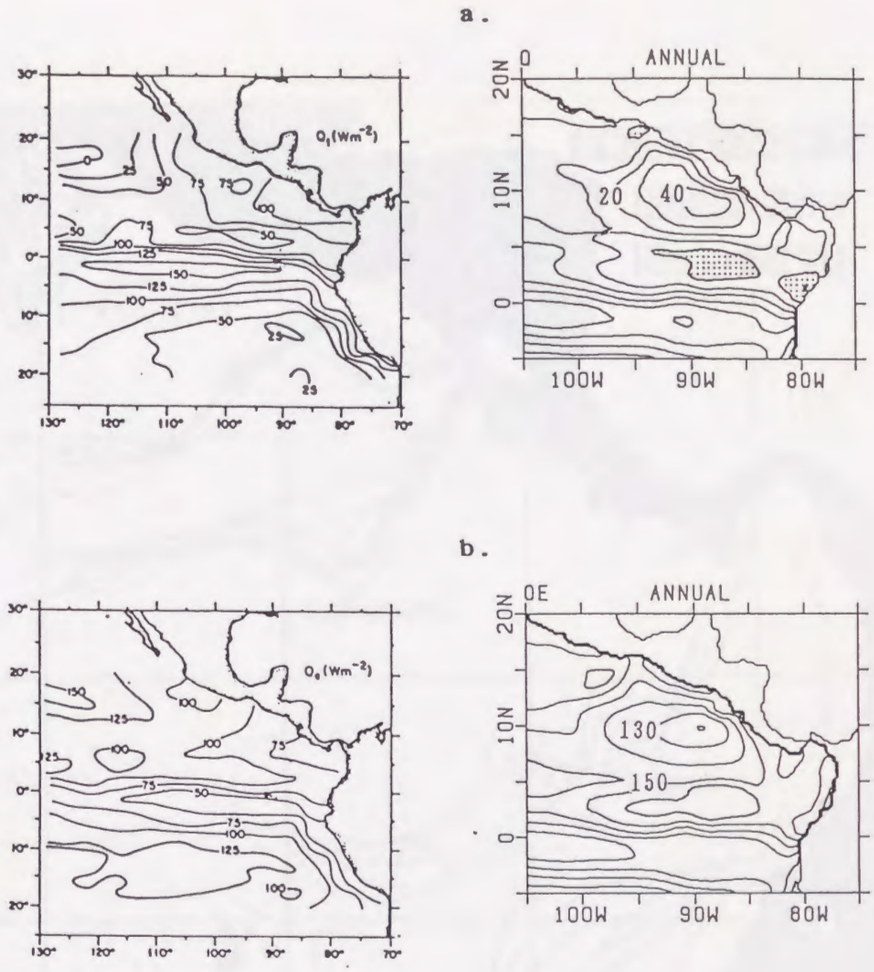


Figure 23: Surface heat flux. (a) Annual mean total downward heat flux. (b) Annual mean upward latent heat flux. Left panel: observations (after Reed, 1985). Right panel: the present model simulation. Contour interval is 25 W $m^{-2}$ (left), and 10 W $m^{-2}$ (right).

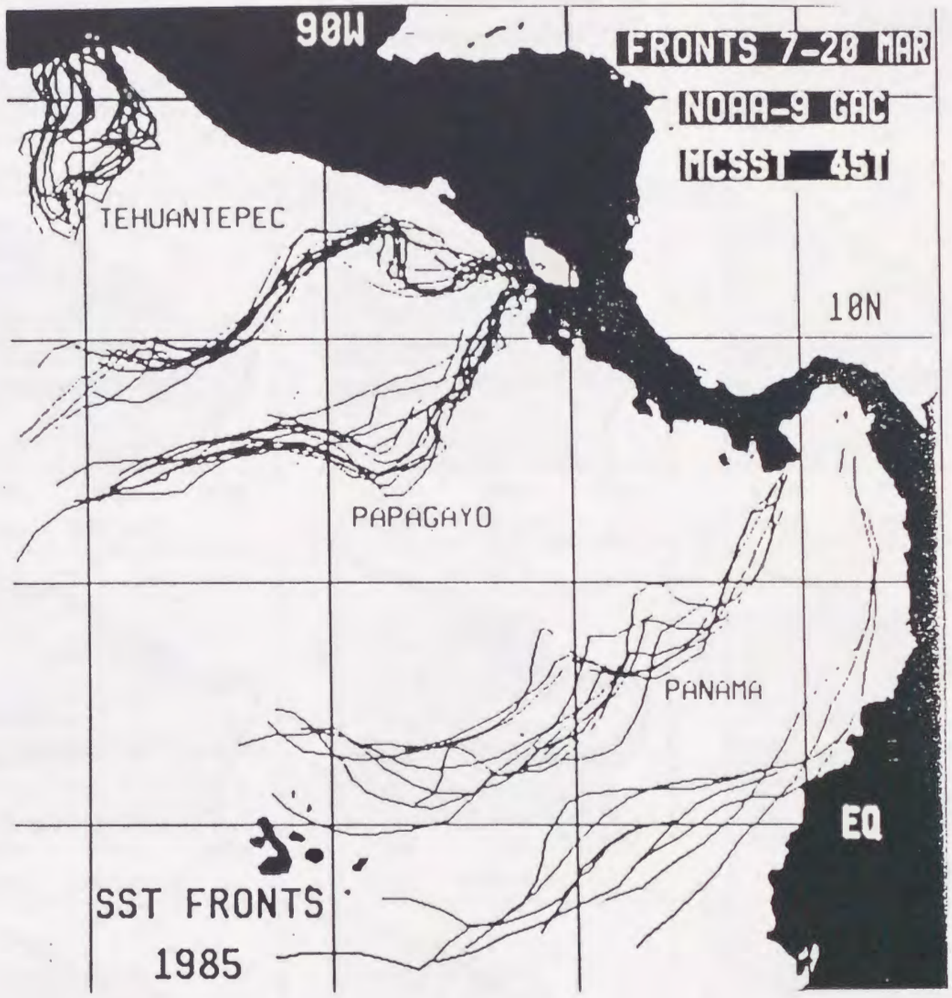


Figure 24: Location of SST fronts from individual SST images leeward of the mountain passes from March 7 to 20, 1985 (after Legeckis, 1988).

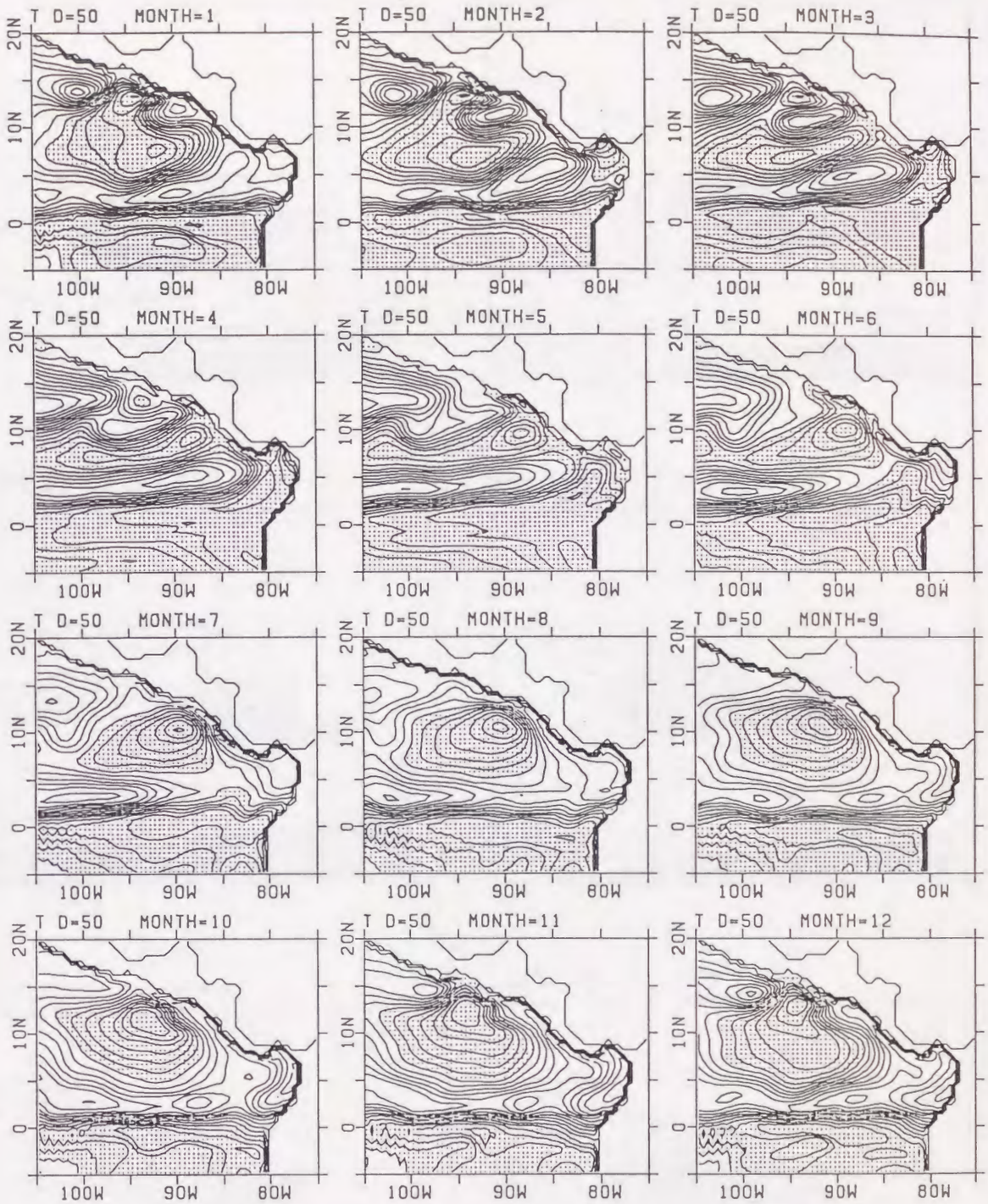


Figure 25: Annual march of subsurface temperatures simulated in a global Pacific ocean model (Masumoto, 1989) at a depth of 50 m.

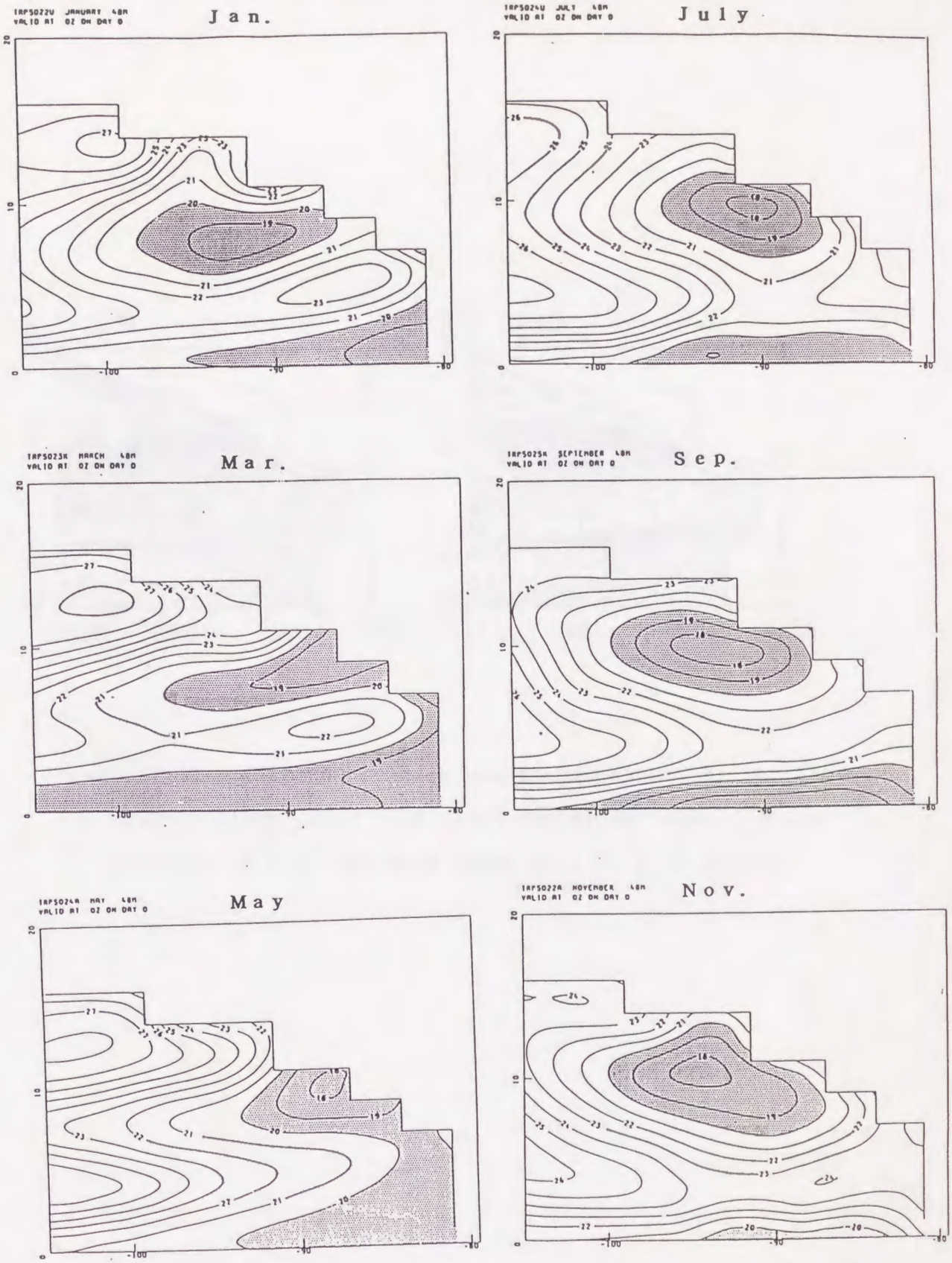


Figure 26: Same as Fig.25 except that the model is another global Pacific model (Gordon, 1990).

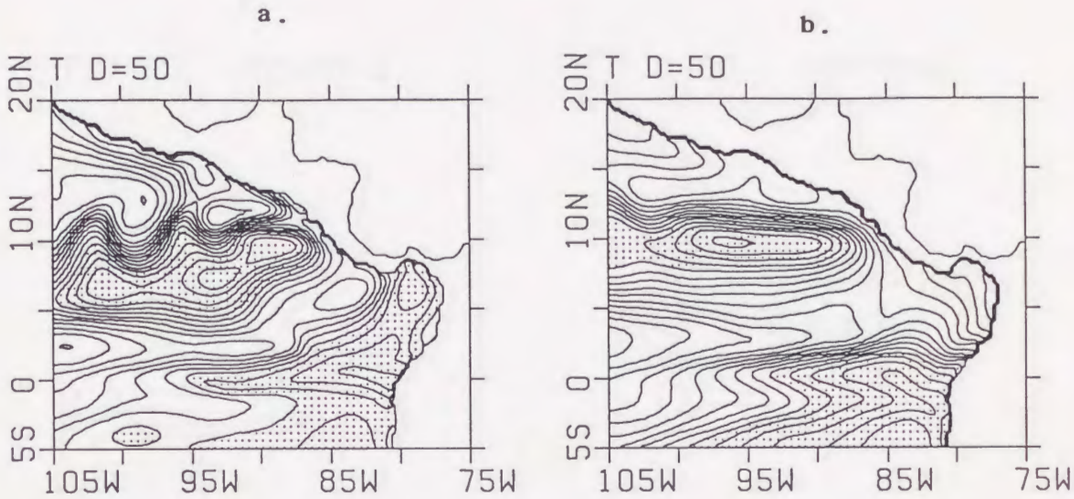


Figure 27: Quasi-steady temperature fields caused by (a) fixed January winds (EX1), (b) fixed May winds (EX2). Contour interval is 1°C. The area lower than 20°C is shaded.

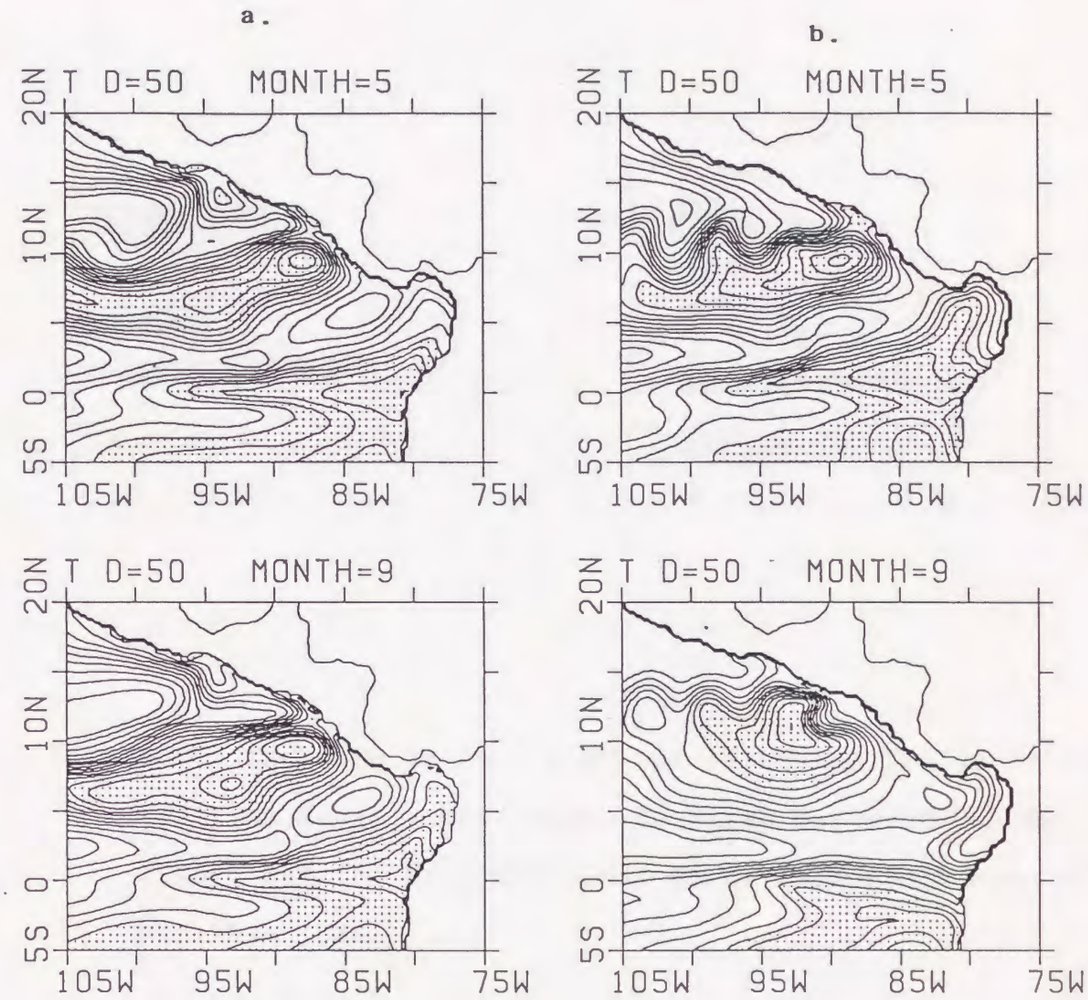


Figure 28: The same as in Fig.27 but with wind fields switching (a) from monthly mean winds to a fixed January wind on January 15th (EX3), and (b) from a fixed January wind to monthly mean winds on January 15th (EX4).

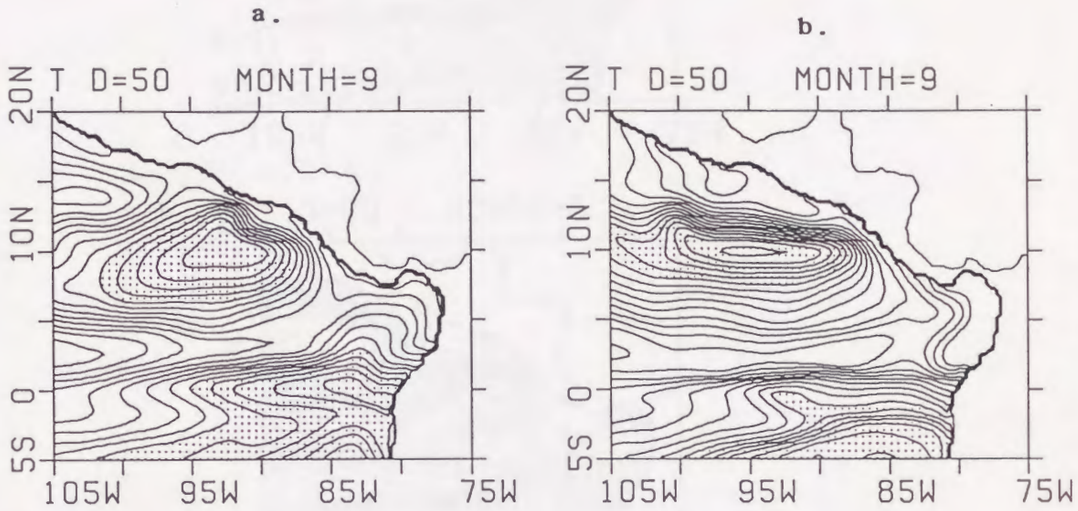


Figure 29: The same as in Fig.27 but with wind fields switching (a) from monthly mean winds to fixed May winds on May 15th (EX5), and (b) from fixed May winds to monthly mean winds on May 15th (EX6).

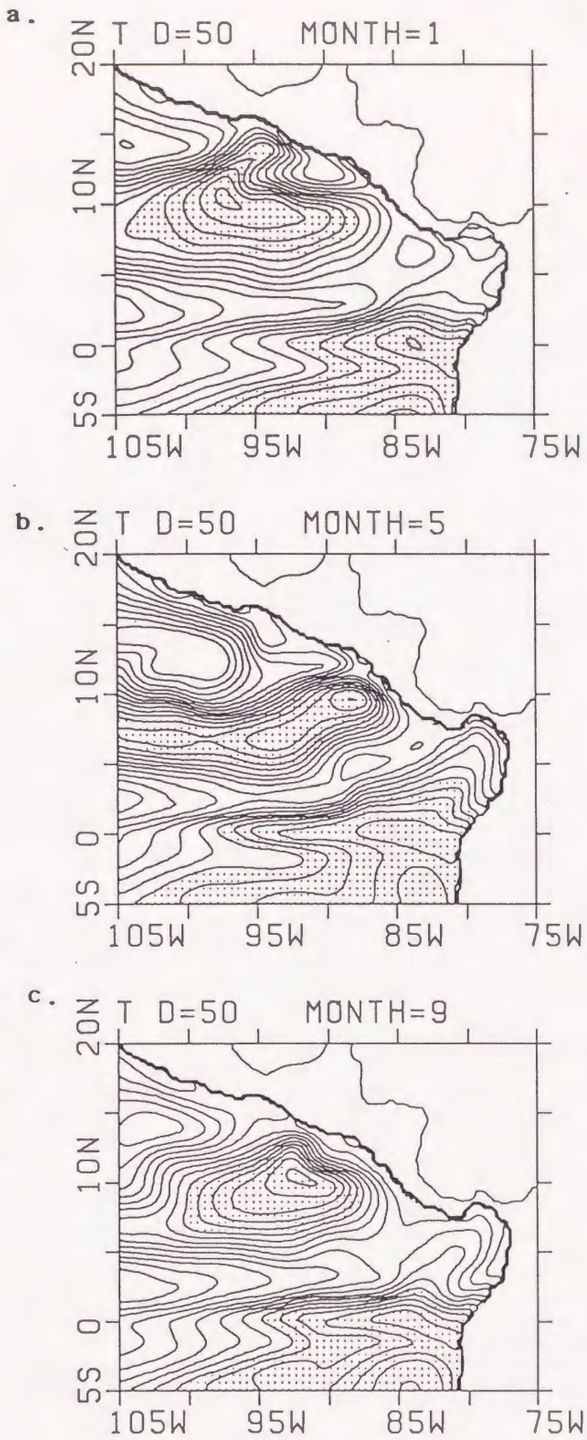


Figure 30: Temperature fields obtained in EX7. The winds are composed of two kinds of wind fields. From January to April the winds are fixed to January winds. From May to December the winds are fixed to May winds. The others are the same as in Fig.27.

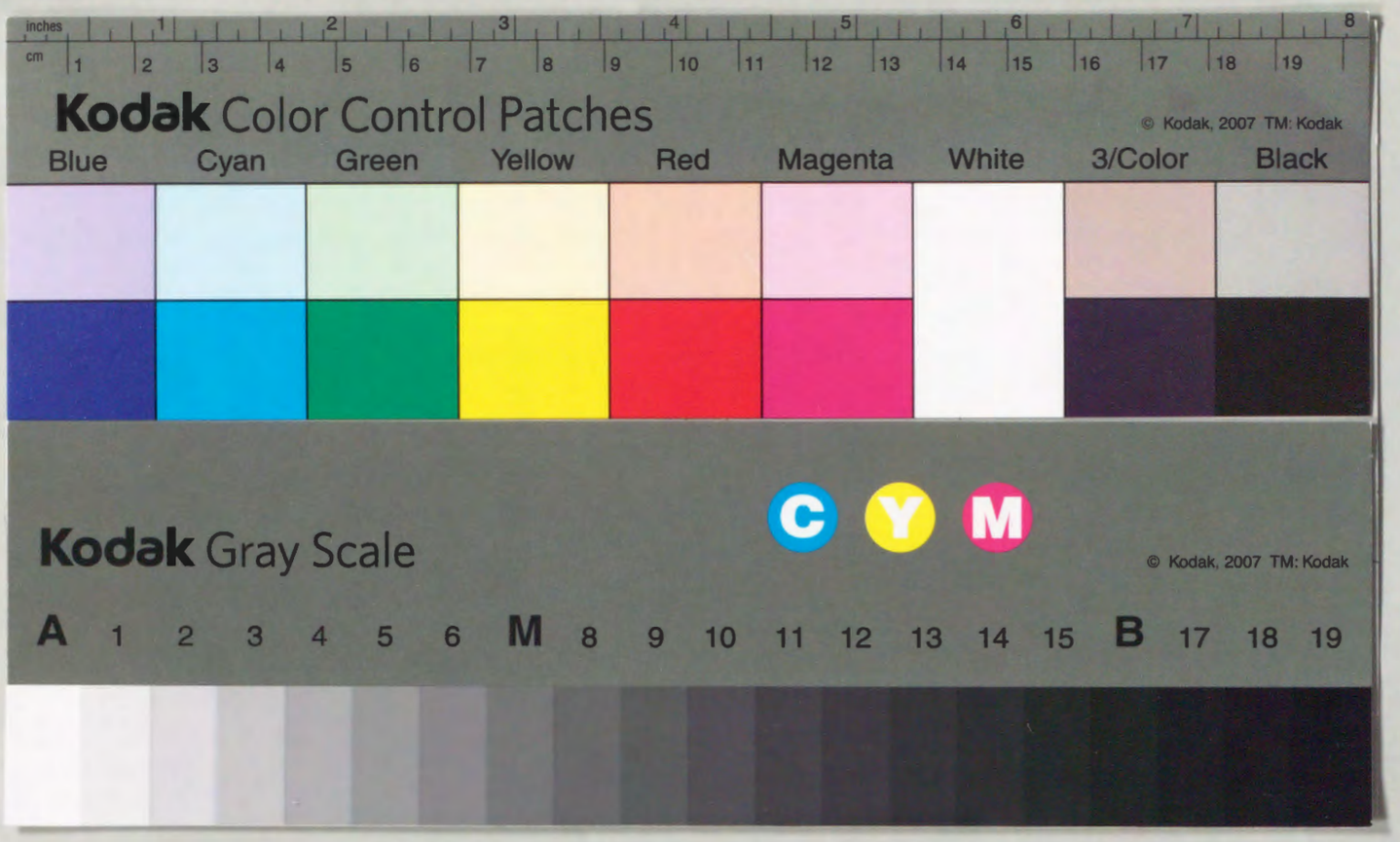
inches
cm
Kodak Color Control Patches
© Kodak, 2007 TM: Kodak
Blue
Cyan
Green
Yellow
Red
Magenta
White
3/Color
Black
Kodak Gray Scale
C
Y
M
© Kodak, 2007 TM: Kodak
A 1 2 3 4 5 6 M 8 9 10 11 12 13 14 15 B 17 18 19